Siting Methodologies for Tidal In-Stream Energy Conversion (TISEC) Systems

Samuel Gooch

A thesis
submitted in partial fulfillment of the
requirements for the degree of

Master of Science in Mechanical Engineering

University of Washington

2009

Program Authorized to Offer Degree:
Mechanical Engineering

University of Washington
Graduate School

This is to certify that I have examined this copy of a master's thesis by

Samuel Gooch

and have found that it is complete and satisfactory in all respects,
and that any and all revisions required by the final
examining committee have been made.

Committee Members:

_____
Jim Thomson

_____
Brian Polagye

_____
Alberto Aliseda

Date_____

University of Washington

Abstract

Siting Methodologies for Tidal In-Stream Energy Conversion (TISEC) Systems

Sam Gooch

Chair of the Supervisory Committee:
Professor Jim Thomson
Applied Physics Laboratory

Tidal In-Stream Energy Conversion (TISEC) is a promising source of clean, renewable and predictable energy. One of the preliminary steps in development of the technology is establishing a standardized and repeatable methodology for the characterization of potential deployment sites. Stationary Acoustic Doppler Profiler (ADCP) velocity data collected at four sites near Marrowstone Island, Puget Sound are used to test the applicability of metrics characterizing maximum and mean velocity, eddy intensity, rate of turbulent kinetic energy dissipation, vertical shear, directionality, ebb and flood asymmetry, vertical profile and other aspects of the flow regime deemed relevant to TISEC. Based on these analyses, the flow at three sites clustered along the east bank of Marrowstone Island (referred to as the "D" sites) are found to be mainly bidirectional and have similar ebb and flood velocities and relatively low levels of turbulent activity. The site near the north point of Marrowstone Island (the "C" site) has higher maximum and mean ebb velocities, but is more asymmetrical and has higher levels of turbulent activity. A two-dimensional "kinematic resource map" is developed for the more promising "D" sites, showing the spatial variation of velocities throughout the area. This map is based on data collected using a vessel-mounted ADCP in linear transects running roughly perpendicular to the flow at the site. Interpolation between these transects along isobaths yields a rough grid of velocities, from which the kinematic resource map can be determined using a two-dimensional interpolation scheme. Results are promising, although this method may not work well at sites with different bathymetric and geographic characteristics. The methods and conclusions are device-neutral, however device specific considerations will be important prior to developing TISEC sites.

Contents

List of Figures

List of Tables

Acknowledgements

I would like to give a sincere thank-you to Dallas, Larry and Mike at Sound and Sea Technology and Dr. Simoncini and the Washington Research Foundation for their financial support, without which this research would not have been possible. Additional thanks to Sound and Sea for making the Marrowstone ADCP data available. I would like to thank Doctor and Professor Jim Thomson for teaching, training and mentoring me in all aspects of this research, and for providing guidance and leadership for the project as a whole. I've learned more in these past eight months than I ever expected I would and for that I am extremely grateful. I would like to thank Professor Brian Polagye for providing tons of insight, on-the-spot-leadership, great edits and much needed engineering and MATLAB advice. I would like to thank Tamara for providing moral support and Pita Pit, and to Alex for providing Dramamine during the August research trip. I would also like to thank Chris Bassett, and apologize for losing the hydrophone data. I would also like to thank Joe Talbert for being cool in general and repeatedly getting the Seaspider back successfully. I would like to thank Professors Aliseda and Horner-Devine for their courses in fluid dynamics, which although sometimes painful at the time have been extremely relevant.

This material is based upon work supported by the Department of Energy under Award Number DE-FG36-08GO18179.

This report was prepared an account of work sponsored by an agency of the United States Government. Neither the United States Government nor any agency thereof, nor any of their employees, makes any warranty, expressed or implied, or assumes any legal liability or responsibility for the accuracy, completeness, or usefulness of any information, apparatus, product, or process disclosed, or represents that is use would not infringe privately owned rights. Reference herein to any specific commercial product, process, or service by trade name, trademark, manufacturer, or otherwise does not necessarily constitute or imply its endorsement, recommendation, or favoring by the United States Government or any agency thereof. Their views and opinions of the authors expressed herein do not necessarily state or reflect those of the United States Government or any agency thereof

Overview

Site characterization is one of the first steps in the development of a Tidal In-Stream Energy Conversion (TISEC) project of any scale. As such, it is also one of the first areas of research undertaken by the University of Washington branch of the Northwest National Marine Renewable Energy Center (NNMREC), a newly formed interdisciplinary group focusing on the advancement of TISEC technology.

This research is based on data from two separate projects, both in Puget Sound. One is a Navy-funded project off the coast of Marrowstone Island, intended to demonstrate the feasibility of TISEC for providing the 25% renewable energy mandated for all defense agencies by the year 2025 [1]. Data from this project are provided by Sound and Sea Technology, a partner of NNMREC. The second is a pilot project in Admiralty Inlet, Puget Sound, undertaken by the Snohomish County Public Utility District (SnoPUD), which is eventually intended to become a utility-scale installation. This will help to fulfill the utility's obligation under initiative I-937 to obtain 15% of its electricity from renewable sources by 2020 [2]. NNMREC has partnered with SnoPUD on the project and is currently collecting velocity and environmental data at the site.

This research is divided into three sections. The first is a literature review covering the current state of TISEC site characterization methodologies and techniques. The second is a collection of metrics specifically tailored to TISEC, based on ADCP velocity data collected at a fixed point over a long (1-3 month) period of time. The third section outlines a methodology for determining the small-scale variability in a site's velocity (in the form of a 'velocity map') using data collected from a vessel-mounted ADCP. The methods and findings of this research are to be published as proceedings of the Oceans 2009 'Marine Technology for our Future: Global and Local Challenges' conference, under the name "Siting Methodologies for Tidal Power".

Part I: Literature Review

Introduction

To date, little literature has been published on methods for field data collection specifically tailored to Tidal In-Stream Energy Conversion (TISEC) site evaluation. Several paper studies have been conducted based on existing tidal current data sources such as the Admiralty Charts in the United Kingdom or the Tidal Current tables published by the National Atmospheric and Oceanic Administration (NOAA) in the Unites States, [3], [4]. Errors in these predictions can be high, as the predictions are based on vintage surveys and were not originally intended for resource assessment [4]. A study conducted by Black and Veatch found discrepancies of as much as 2 m/s at a site using different tidal atlases [3]. For this reason, field velocity data collection for TISEC site analysis is widely accepted as a necessity, and is a component of all but the first stage of the European Marine Energy Centre's (EMEC) site selection methodology, the only standard procedure proposed on this topic to date [5]. The following literature review will cover existing methods for processing velocity data at potential TISEC sites, including an overview of Acoustic Doppler Current Profiler (ADCP) technology, widely regarded as the standard for field velocity data collection [6].

Importance of Site Characterization

Velocity data is critical in evaluating a site for TISEC devices, as current speeds are the primary factor in determining the quality of a potential site [7]. Power density scales with the cube of velocity, so even a modest increase in velocity can lead to significant gains in production [8]. Velocity time series data allow for the calculation of additional metrics (e.g., velocity distribution and tidal ellipses), yielding a more in-depth understanding of the tidal dynamics at a site. Velocity data are also used for calculating the maximum forces and stresses that a device

may need to withstand, useful for design considerations [5]. These topics are covered in depth later in this review.

Additionally, EMEC guidelines and a study conducted by Puget Sound Tidal Power both use field velocity data for the calibration of computational fluid dynamic (CFD) models of the area [5], [9]. Field velocity data is also the only basis for performing turbulence calculations, which is critical for the design and siting of TISEC devices and foundations [10].

ADCP Background

While Tidal In-Stream Energy Conversion (TISEC) is an emerging technology, much of the instrumentation used to characterize potential sites is mature and commercially available. The Acoustic Doppler Current Profiler (ADCP) is the primary instrument for collecting velocity data and has been the industry standard since the early 1980's [6]. ADCP units can be deployed as stationary units on the seafloor, moored on the surface, or installed on a moving vessel depending on the device configuration and the type of data required [11]. A stationary ADCP deployment will give a continuous record at a fixed location, whereas a shipboard survey will give information as a function of time and location. ADCPs measure water velocity using the Doppler effect by transmitting sound at a fixed frequency and listening to echoes returning from sound scatterers in the water. These sound scatterers are small particles or plankton that reflect the sound back to the ADCP [11]. When sound scatterers move away from the ADCP, the reflected sound is Doppler-shifted to a lower frequency proportional to the relative velocity between the ADCP and scatterer. The backscattered sound then appears to the ADCP as if the scatterers were the sound source. Therefore, the ADCP hears the backscattered sound Doppler-shifted a second time, since the unit both sends and receives the signal. This allows an ADCP unit to perceive how particles are moving parallel to the signal sent by the

ADCP transducer (the unit sending and receiving the signal). However, with only one transducer only this one velocity component can be determined. In order to determine velocities in a 3 dimensional Cartesian coordinate system, 3 transducers are required. These signals do not need to be orthogonal, as they can later be rectified using trigonometry, but they do need to be aligned at different angles in order to capture separate directional components of the velocity [11]. The Doppler shift is calculated as a series of ranges from the transducer by knowing the travel-time of the signal, and the result is a set of vertical "velocity profiles" giving a quantitative description of the current speeds as a function of depth at a specific time and location. Different ADCP packages are available for different uses. ADCP units that operate at high frequencies (over 1000kHz) are capable of producing higher resolution velocity profiles, although their range is much smaller because of increased sound absorption. The reverse is true for low frequency (less than 200kHz) units.

ADCP Deployments

The first round of field data collection proposed by the EMEC guidelines is a boat-mounted survey consisting of transects at the proposed TISEC site, which provides an overview of the spatial velocity variability at a site and is of use for determining some of the most important tidal harmonic constituents and calibrating hydrographic models. EMEC recommends that these surveys be conducted twice, both at the peak of a spring (strong) tide. Transect data to be collected includes time, location (latitude and longitude in WGS 84 [12]), velocities in the three directions, signal to noise ratio (SNR) for the three directions, temperature, pressure, vertical survey range, average velocity magnitude and direction, quality indicators and confidence levels for the horizontal positioning of the vessel [5].

After the transect survey, EMEC guidelines call for a stationary ADCP deployment. The report recommends a minimum of 3 months velocity data for a TISEC array, or 15 days worth for a single device. The guidelines recommend a minimum of two ADCPs be deployed for redundancy. A study of currents in the Tacoma narrows used 30 days worth of data from three units as it was the minimum required for the calibration of their CFD model [9]. Another document published by EMEC recommends that stationary ADCP deployments last for a minimum of 30 days, which allows for harmonic decomposition of the tidal signal, explained in depth on page 9.

EMEC recommends that as an additional step, velocity data be collected for up to a year once a TISEC deployment site has been pinpointed. Stationary data collected under EMEC guidelines includes velocities in the three directions, standard deviation in the three directions, signal to noise ratio (SNR) for the three directions, temperature, pressure, cell start depth (bottom cell) and cell stop depth (top cell), average velocity with direction, and turbulence intensity (where applicable) [5]. It should be noted that any turbulence calculations will require data of higher resolution than that proposed under the EMEC long term deployment guidelines [10].

Several parameters must be configured for any ADCP deployment, including pings per averaging interval (ensemble), depth cell (bin) size, and ensemble duration [11]. In any deployment configuration, the tradeoffs must be considered between range, resolution and random noise, as shown in Figure 1. Smaller bin sizes create higher resolution velocity profiles, although pulse length is shorter and deviation will increase. Fewer pings per ensemble will also increase deviation, although ensemble duration will decrease and higher temporal resolution output will be possible.

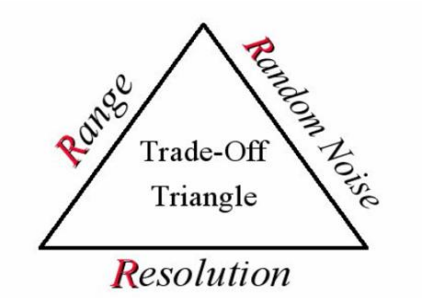

Figure 1. Trade-off triangle showing relationship between range, random noise and resolution [11].

Additionally, stationary ADCPs are generally stand-alone units and are constrained by the amount of power available (battery size) or by data storage limitations. Keeping these restrictions in mind, stationary ADCPs are generally configured for long deployments at low temporal resolutions suitable for capturing mesoscale currents activity or for short deployments using rapid sampling schemes suitable for eddy intensity and turbulence characterization [10].

Transect surveys are generally not constrained by data storage or power, but are limited by the speed at which an acoustic signal can reach the seafloor and return to the vessel [11]. EMEC recommends that transects last less than 10 minutes each, which sets a limit on the maximum possible length, as vessel speed is also capped to maintain good correlation [11]. EMEC has established some preliminary guidelines for ADCP deployments aimed at TISEC site characterization, shown in Table 1.

Table 1. EMEC Guidelines for TISEC ADCP deployments.

	Velocity Characterization [5]	Turbulence Characterization [10]	Transect (Mobile) Survey [5]
Time/ping [s]	0.5	1	0.5
Ensemble Interval [s]	240-1200	1	1
Duration [days]	15+	5	<10 minutes/transect
Bin Size [meters]	0.5-1	1	1
Referential Coordinates	Cartesian (Transformed)	Beam Coordinates (Untransformed)	Cartesian (Transformed)
First Bin	"As close as possible to seafloor"	1 meter	Less than 5 meters below surface

Data Analysis: Metrics Proposed By EMEC

This section describes the metrics proposed by the EMEC guidelines for tidal resource assessment [5], as well as additional background information where available.

Velocity Distribution

A velocity histogram is proposed for visualization of the probability of discreet velocities at a site, as shown in Figure 2. 10 minute intervals and 0.1m/s bins are recommended. This analysis is useful for comparing velocity distributions at different locations within a given project area, and can also be used to predict the amount of time velocities at a site will exceed a minimum "cut in" speed and a TISEC device will produce power.

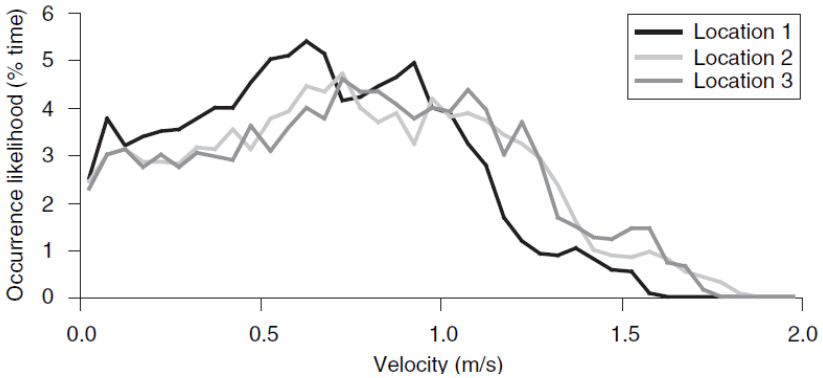

Figure 2. Velocity distribution histogram shown using data collected at three different locations at the EMEC testing facility using 10 minute averaging intervals and 0.1 m/s bins [5].

Maximum Velocities

The maximum velocity is defined as the peak velocity that has been reached for 10 minutes during an entire month. If data from a transect survey is used, the velocity averaged over the entire transect is to be used, as the surveys are to be conducted during the spring tides and should therefore represent the highest velocities of the month. This value is to be reported either at the hub height of a TISEC device or averaged over the entire water column.

Tidal Range

This is the range in depths throughout a tidal cycle from high tide to low tide.

Power Density

Power density scales with the cube of velocity and therefore highlights the importance of strong currents [7]. The average power density can be expressed with the equation

$$P = \frac{1}{2}\rho\langle v^3\rangle \tag{1.1}$$

where the brackets indicate an average. This is the flux of kinetic energy density $1/2\rho v^2$ through a cross-sectional area. Note that the 10-minute velocity

ensembles are used as opposed to a long-term average velocity value, as the average must be taken after cubing the velocities.

Harmonic Analysis

The periods of motion of the earth, sun and moon are fixed, and as a result, so are the periods of the tidal forcing their movements produce. Newton's static theory of equilibrium tide referred to these as *partial tides,* each identified by a unique and known period of oscillation, and each representing a specific solar or lunar tractive forcing. The dynamic theory of Laplace states that partial tides can be applied as a series of sine waves of known frequency which can be summed to reproduce the actual tidal behavior. In addition to a fixed period, each of the partial tides (known as *tidal constituents*) has an amplitude and phase. The harmonic method of tidal analysis, credited to Lord Kelvin, is based on the extraction of these constituents from the power spectra of the observed tidal signal [13].

The predominant constituent, except in areas with mainly *diurnal* tides (one low and one high tide per day), is the *main lunar semidiurnal* or M_2 constituent, with a period of 12.42 hours. The main solar constituent, S_2, has a period of 12.00 hours. "M" and "S" refer to the moon and the sun, and the "2" subscript refers to the fact that the periods are semidiurnal, or having two tidal cycles per solar or lunar day. When superimposed, the two constituents initially appear to be in phase. However, after a period of 14.76 days, the two constituents will be exactly out of phase. This oscillation is known as the *spring-neap cycle.*

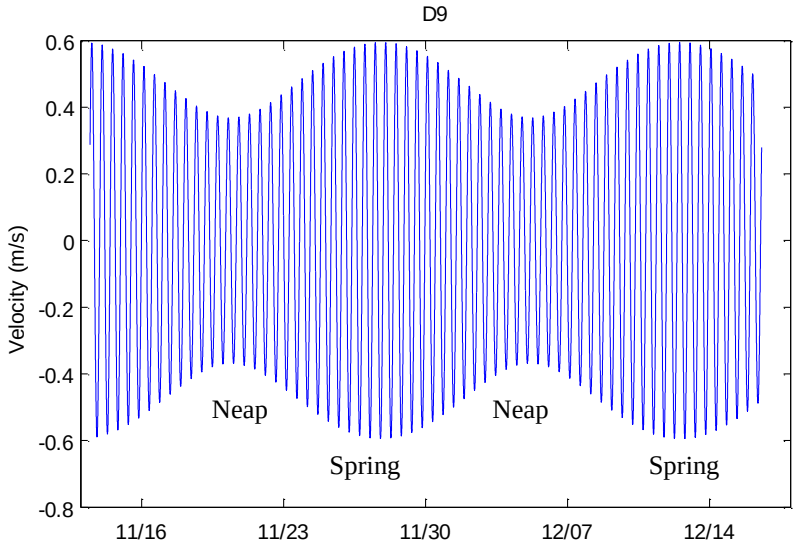

Figure 3. Spring-neap tidal cycle at Marrowstone site D9.

Adding the *larger lunar elliptic semidiurnal* or N_2 tidal constituent incorporates the perigean-apogean cycle, caused by the ellipticity of the moon's orbit during the 27.55 day elliptic month. Adding the K_1 and O_1 constituents incorporates the diurnal *tropic-equatorial* cycle. The behavior of these constituents is shown in Figure 4 [13].

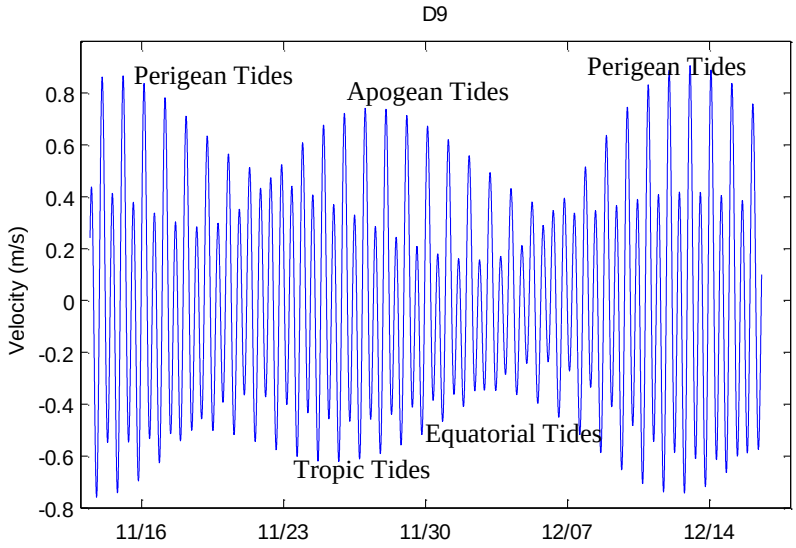

Figure 4. Tidal cycles produced by the M_2. S_2, N_2, K_1 and O_1 constituents at Marrowstone site D9.

The aforementioned tidal constituents can also be used to describe the type of tide, whether it is semidiurnal, diurnal, or a mixture of the two. This is commonly defined using a tidal form number, expressed as [13]:

$$Tidal\ Form\ Number = \frac{K_1 + O_1}{M_2 + S_2} \tag{1.2}$$

If the tidal form number is less that 0.25, the tides are semidiurnal. Form numbers between 0.25 and 1.5 are mixed mainly semidiurnal. Form numbers between 1.5 and 3.0 are mixed mainly diurnal, and above 3.0 are considered diurnal. Example tidal signals and locations in which they occur are shown in Figure 5. Harmonic analysis can be performed on data using freely available code such as the *T_tide* package for MATLAB [14].

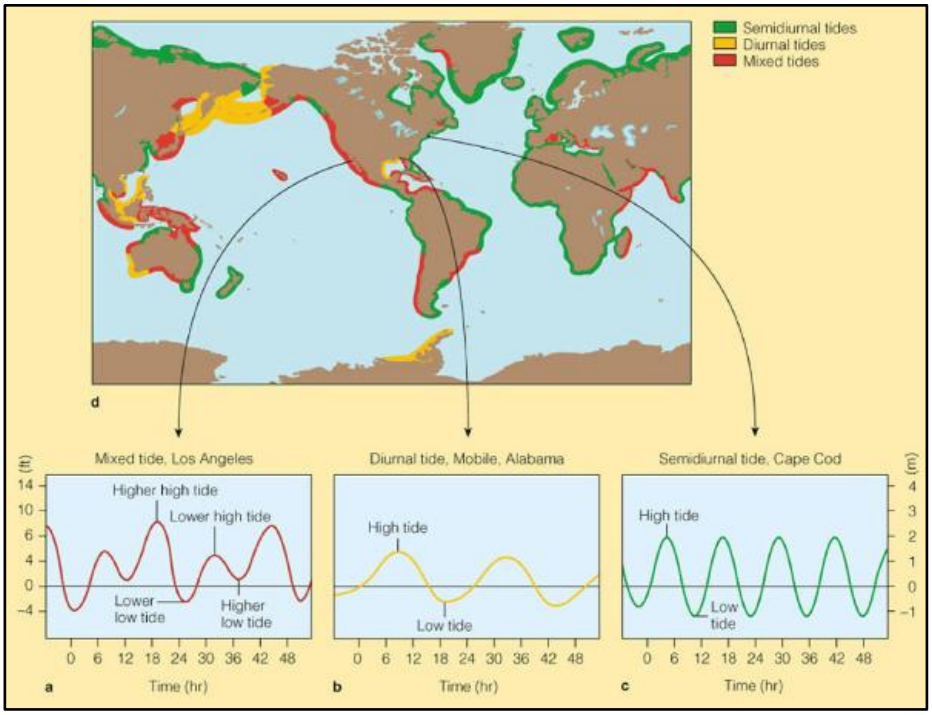

Figure 5. Types of tide and locations in which they occur. © Brooks/Cole, Cengage Learning

While only five constituents have been described thus far, their behavior typically accounts for over 75% of tidal activity. The five most predominant constituents are shown in Table 2, although over 400 constituents have been identified [14].

Table 2. Tidal Constituents in Standard Order [5], [13].

Common name	Period (hours)	Rank	Full name
M_2	12.42	1	Main Lunar Semidiurnal
S_2	12.00	2	Main Solar Semidiurnal
N_2	12.66	3	Larger Lunar Elliptic Semidiurnal
K_1	23.93	4	Lunar-Solar Declinational Diurnal
O_1	25.82	5	Lunar Declinational Diurnal

EMEC guidelines state that for later stages of site characterization at least 20 tidal constituents should be resolved, and it should be possible to extract a minimum of 23 tidal constituents using one month of velocity data [5]. It should be noted that while it may technically be possible to extract this many constituents, only a few may have a signal to noise (SNR) ratio high enough to justify their inclusion in a long term prediction. Including additional constituents will likely lead to characterization of noise in the tidal signal, and will actually decrease the quality of the prediction [13]. Additionally, some regionally important constituents may be convolved with others (e.g. K_1 and P_1 in Puget Sound, Washington) because their periods are extremely similar, and will require longer timeseries to determine. A study by Lueck and Lu found that 91% of the flow velocity at a test site in the Cordova Channel, British Columbia could be explained using only the M_2, S_2, K_1 and O_1 constituents [15]. In an example presented by Pawlowicz et al. in [14], a harmonic analysis of a 66 day tidal elevation series found only 11 constituents had a SNR higher than one, and only 6 had a SNR higher than two. Further, tidal elevation series are generally easier to predict than velocity series. Much of the tidal signal not explained by these few predominant constituents is

generally due to non-tidal variations caused by weather, turbulence, local bathymetric influence or baroclinic circulation and cannot be predicted using harmonic analysis [13].

EMEC recommends an extrapolation of field data to a period of one year using harmonic analysis and comparing the power density given by the two distributions. If the power density differs by more than 5%, explanation is recommended as to the causes of the variation, as this could indicate that data taken at a site is not representative of overall activity [5]. However, as explained previously, variations due to weather cannot be predicted using harmonic analysis and could explain differences between extrapolated and field datasets [13]. EMEC guidelines recommend analyzing this difference between harmonic tidal predictions and actual field data to estimate the effects of metorological phenomena [5].

Tidal Ellipse

While, in theory, tidal currents are perfectly bi-directional, in practice ebb and flood currents are two-dimensional in nature and cannot be described as a simple back-and-forth motion. This is in contrast to tides, described as a one-dimensional height difference from a reference datum [13]. Currents may be offset by less than 180˚ and/or the direction of the currents may vary throughout the tidal cycle. The tidal ellipse is defined as the path the currents trace out during one period for a given tidal constituent. Figure 6 shows a simple tidal ellipse with the major and minor axes labeled. For TISEC considerations, a tidal ellipse with a large major and small minor axis is ideal, as this represents a strongly bi-directional flow. This becomes important for devices that may not be able to extract energy from all directions, such as those with no or limited ability to yaw into the direction of the currents. A device with no yaw control would be

aligned parallel to the major axis. Figure 7 shows tidal ellipses of the M_2 currents throughout one 12.4 hour period in Monterey Bay.

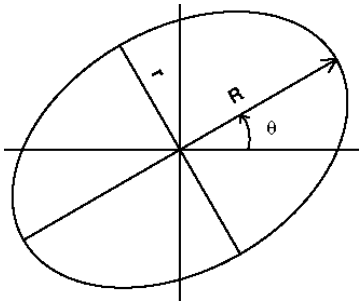

Figure 6. Tidal Ellipse with major axis (R), minor axis (r), and orientation θ. This tidal ellipse traces the direction and magnitude of the currents throughout one period of the constituent it describes [16].

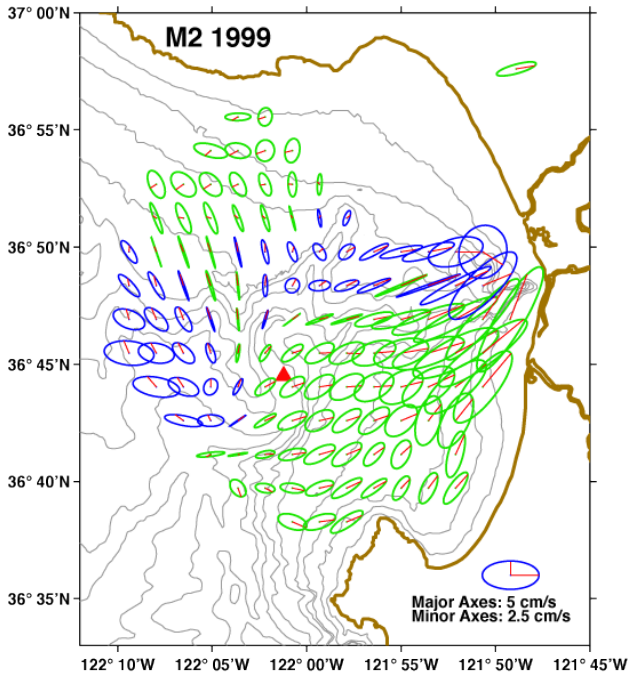

Figure 7. M_2 surface current tidal ellipses for Monterey Bay. The red lines indicate the direction at which the current is pointing at a given time. The blue ellipses indicate a counterclockwise rotation; the green ellipses indicate a clockwise rotation [16].

EMEC guidelines recommend generating separate ellipses for ebb and flood tides, and if the flow direction is off of the major axis by more than 10% for over 5% of the time, a directionality offset in the available resource is to be applied if applicable to the functionality of a specific TISEC device. However, it is somewhat unclear as to what separate flood and ebb ellipses entail, as both tides are necessary for the construction of a single ellipse. This metric may not be relevant if a device is able to extract energy from any direction, but should still be considered for the purpose of support structure and yaw tracking.

Turbulence

EMEC has reserved a section for studies of turbulence in its guidelines, but has not established its own specifications to date, instead recommending that recent papers on the topic be consulted [5].

Turbulence is related to the formation of eddies of many different length scales. The majority of the energy is contained in the largest structures. Through largely inviscid mechanisms, the largest eddies "cascade" their turbulent energy to smaller structures and so on, until the eddies reach a point at which viscous dissipation becomes predominant. This is known as the Kolmogorov length scale, and at this point the energy contained in the eddies is dissipated into heat [17].

A more recent ADCP survey conducted at the EMEC test berth focused on defining turbulence at the site. The ADCP was configured with 1m bins in the vertical and 1 second sampling. The study focused on turbulence due to the bottom boundary layer and its vertical penetration. "Turbulent" conditions were defined as any sample having a 1m/s difference between maximum and minimum velocities within a centered 10 minute sample [10]. A simple metric from the wind energy industry, termed turbulent intensity, uses the ratio of velocity anomalies to the steady background velocity, where "steady" conditions are generally 10-15 minute samples where mean velocity can be considered constant [18], [19].

More rigorously, treatment the rate of turbulent kinetic energy (TKE) dissipation may be estimated. A recent paper by Wiles et al. [19] describes a method for determining the rate of TKE dissipation at the Kolmogorov scale using data collected from a standard stationary ADCP unit. Other methods for estimating TKE dissipation rates, using variance and spectral techniques, can also be applied to ADCP data [20], [21].

Modeling and Data Comparisons

One of the primary uses of field ADCP data in the EMEC guidelines is model validation and calibration. No particular model is suggested, although a list of possible hydrodynamic models is included. It is specified that the model shall be either 2D or 3D, and information including boundary conditions, frictional parameters and forcing conditions shall be included with proper justification. Once the model has reached equilibrium (this can take 3-5 model days depending on the domain size), the model is to be run for the same length of time as the stationary field survey (nominally 30 days), and results are to be calibrated to the field data [5].

Modeling efforts at the National Northwest Renewable Energy Center (NNMREC) have focused on the Stanford Unstructured Nonhydrostatic Terrain-following Adaptive Navier-Stokes Simulator (SUNTANS) code developed at Stanford for developing a model of Puget Sound [22]. This is a 3D, unstructured grid model that will also be calibrated with ADCP data from Admiralty Inlet, a site with potential for TISEC development shown in Figure 8. The model is non-hydrostatic and is designed to accurately represent vertical fluid movements that might be lost otherwise. Current efforts with the model include matching vertical structure and amplitude changes across Admiralty Inlet [23].

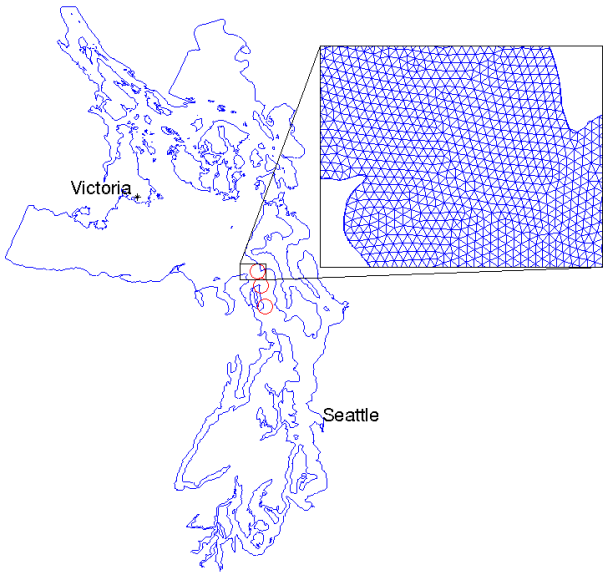

Figure 8. Map of Puget Sound with SUNTANS grid shown at Admiralty Inlet in inset. Potential development sites are shown in red circles [23].

Boundary Layer

EMEC guidelines recommend plotting the depth profile from stationary field data, transect data, and the output of the hydrographic model and comparing the results with depth velocity distributions using formulae commonly employed in industry. A power law approach is employed in the wind energy industry for approximating velocity reduction due to drag within the boundary layer:

$$V = V_0 \left(\frac{z}{d}\right)^{\frac{1}{\alpha}} \tag{1.3}$$

where d represents the total depth, z is the depth at which the velocity is to be approximated, and α is an empirical constant, nominally 7 [24]. EMEC recommends using 10 as a value for α, which results in a steeper curve and therefore smaller boundary layer. Another approximation was developed in the JOULE 1996 resource study, and is shown in Figure 9. These approximations can be used in conjunction with 2D models giving depth-averaged to estimate the velocity at the working height of a TISEC device.

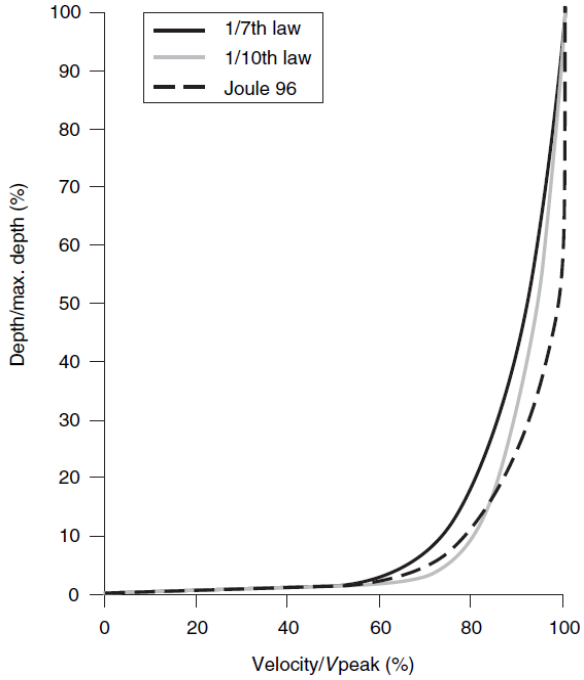

Figure 9. Comparison of boundary layer approximations [5], [25].

Data Analysis: Additional Metrics

A paper by Lu and Lueck [15] describes several other metrics used to characterize ADCP data. These metrics serve to characterize a site beyond the recommendations of the EMEC guidelines and are potentially useful for TISEC site analysis. Some results of their analyses on the Cordova Channel, British Columbia are shown in Figure 10 and Figure 11. These metrics include information about vertical shear, transverse flows, and directional variation as a function of height and time.

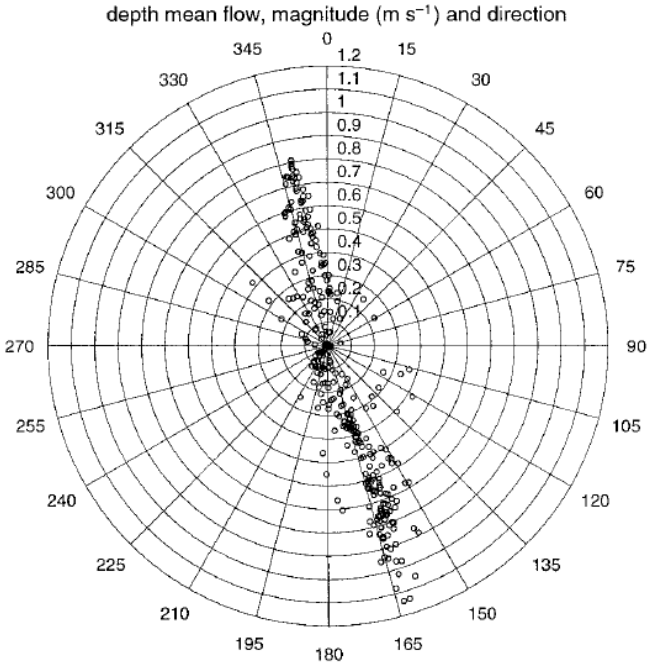

Figure 10. Mean flow magnitude and direction for entire dataset [15].

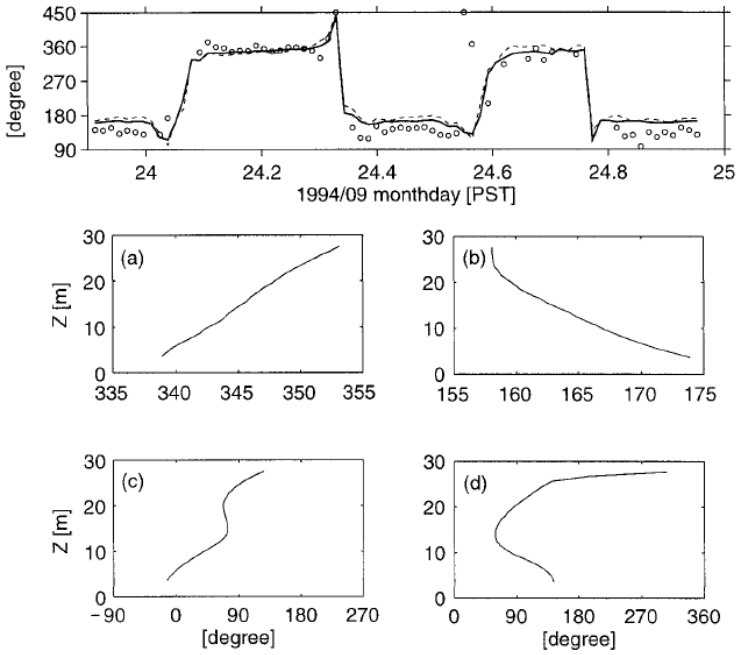

Figure 11. (upper panel) Time series of the direction of the 20-min mean velocity at 3.6m (solid line) and 27.6m (dashed line) and the shear at 3.6m (circles). (lower panels) Typical profiles of current direction during (a) flood and (b) ebb and of the shear direction during the (c) flood and (d) ebb [15].

Part II: Stationary Data Analysis

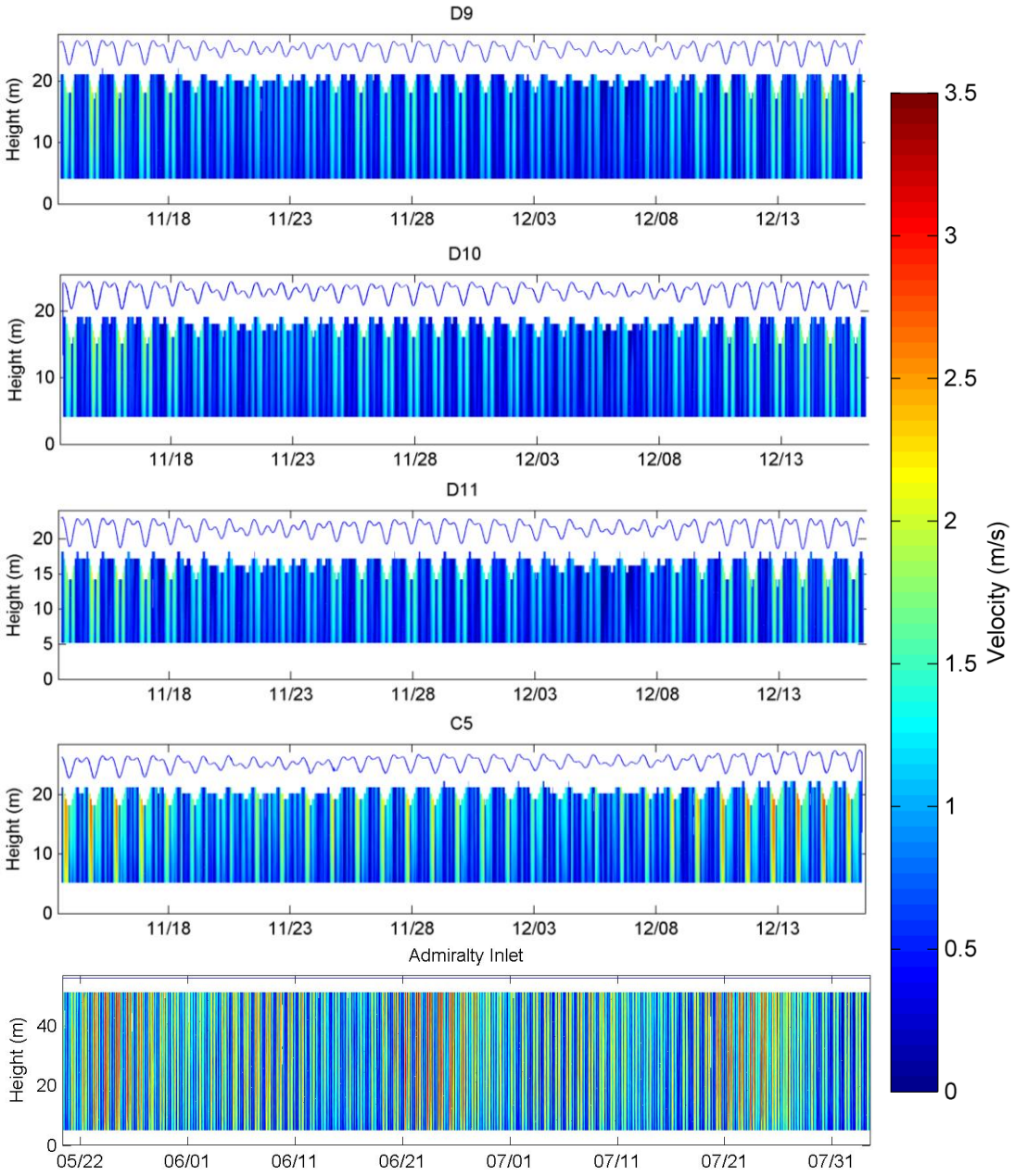

Figure 12. Velocity data at the four Marrowstone sites and at Admiralty Inlet. The blue line indicates surface height. Note that the Admiralty data does not include surface height and is truncated at 56 meters.

Introduction and Device Neutrality

This chapter presents a methodology to characterize potential sites for tidal power development by analyzing Acoustic Doppler Current Profiler (ADCP) data collected at fixed locations, shown in Figure 12. Thus far, site evaluation methods have been developed by private industry and are considered proprietary. Because these methods are not subject to public or peer review, it is difficult to determine whether they are accurate, relevant or repeatable at future sites. Here, a standardized suite of publicly available measurement and analysis methods is developed, which can be used to characterize sites so that they may be directly and fairly compared against one another. These methods utilize repeatable metrics that allow for future sites to be judged not only on the quantitative results of the metrics themselves, but by a relative comparison with similar sites. The methodology developed herein is applied as a test case to several test sites. Four of these sites are under consideration for a Navy demonstration project off the coast of Marrowstone Island, Puget Sound (Figure 13). This data was collected by Orders Research Associates (OARS) and represents the four most promising sites based on mobile velocity data collected by Evans-Hamilton [26]. A fifth site under development by the Snohomish County Public Utility District (SnoPUD) lies near Admiralty Head, Puget Sound (Figure 13). Data collection by the NNMREC is currently underway for this project.

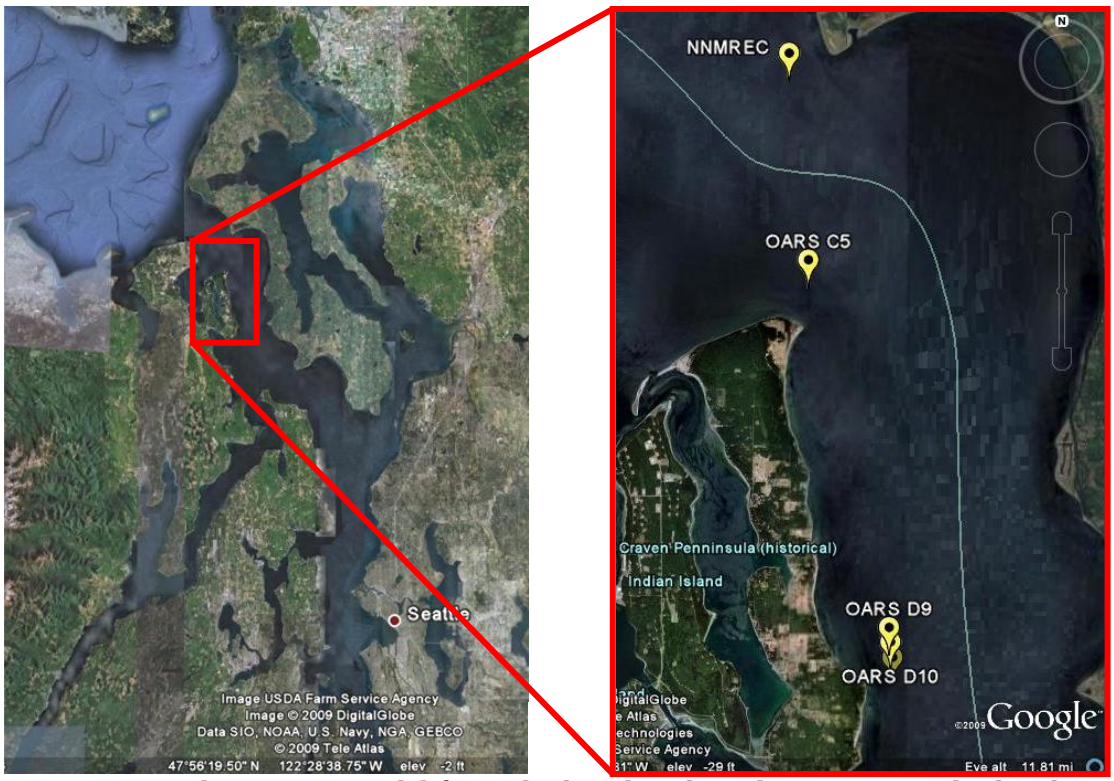

Figure 13. Northern Puget Sound (left) , and Admiralty Inlet and Marrowstone Island (right), with stationary ADCP locations shown in as yellow markers [26]. "NNMREC" location is hereto referred to as the Admiralty Inlet site. Images © DigitalGlobe 2009, © TeleAtlas 2009

When required, a hub height of half the water column depth is assumed. For the four (D9, D10, D11, C5) sites of the Marrowstone Island case study, this is approximately 13 meters, and is calculated using the free surface height as recorded by the ADCP pressure sensor. Hub height at the Admiralty Inlet site is 27.8 meters. Actual hub-height values are tabulated in the Summary of Results (Table 4) at the end of the chapter.

Most metrics are separated into values for ebb, slack, and flood, using a threshold of 0.5 m/s. Ebb and flood regimes are determined using a principal axis decomposition as described in the section on Directionality on page 34. The threshold can be considered an effective "cut-in" speed, but, again, is intended to be device neutral and is well below the actual "cut-in" of all known devices [27].

More importantly, the separation of ebb-slack-flood regimes ensures that the metrics presented are not biased by measurements of no practical importance, such as the fluctuations in velocity direction surrounding slack water. "Summary" statistics reported in Summary of Results (Table 4) on page 48 are an average of the corresponding flood and ebb statistics, weighted by the number of samples in the ebb and flood regimes.

Analysis presumes that the method of power generation would be in-stream (i.e., hydrokinetic), but nothing further is assuming regarding device specifics or performance. In practice, device specifics will be essential in site development decision-making. However, a device neutral methodology is necessary for world-wide site characterization, and that is the focus herein.

Finally, the analysis presented is sensitive to the sampling scheme used. For consistent results, at least 28 days of fixed ADCP data at 1 min intervals and 1 m resolution are required. Most ADCP manufacturers provide deployment software to assist in configuration and specification of memory and power needs to meet the recommended sampling.

All analysis is performed in the MATLAB programming environment.

Data Overview

Full velocity profiles at the five sites for all heights are shown in Figure 12, with the surface height shown as a blue line. Note that surface height is not yet available for the Admiralty Inlet site. The top four bins are truncated at each site, as these are contaminated with noise from wave and wind interactions. Velocities are highest near the surface, as water nearer to the seafloor is more affected by bottom boundary layer drag. While these plots are a convenient way to visualize all data at the same time, examining a single bin is often more practical. Figure 14 shows a one-month timeseries of each site at hub height, in which a two neap

tides surrounded by three partial spring tides can be observed for the four Marrowstone sites. The Admiralty site begins and ends on a neap and contains two springs. Also of interest is the strong ebb on the C5 site, which is largely due to the headland effect of the nearby Marrowstone point (Figure 13) which causes flow acceleration in that direction [28].

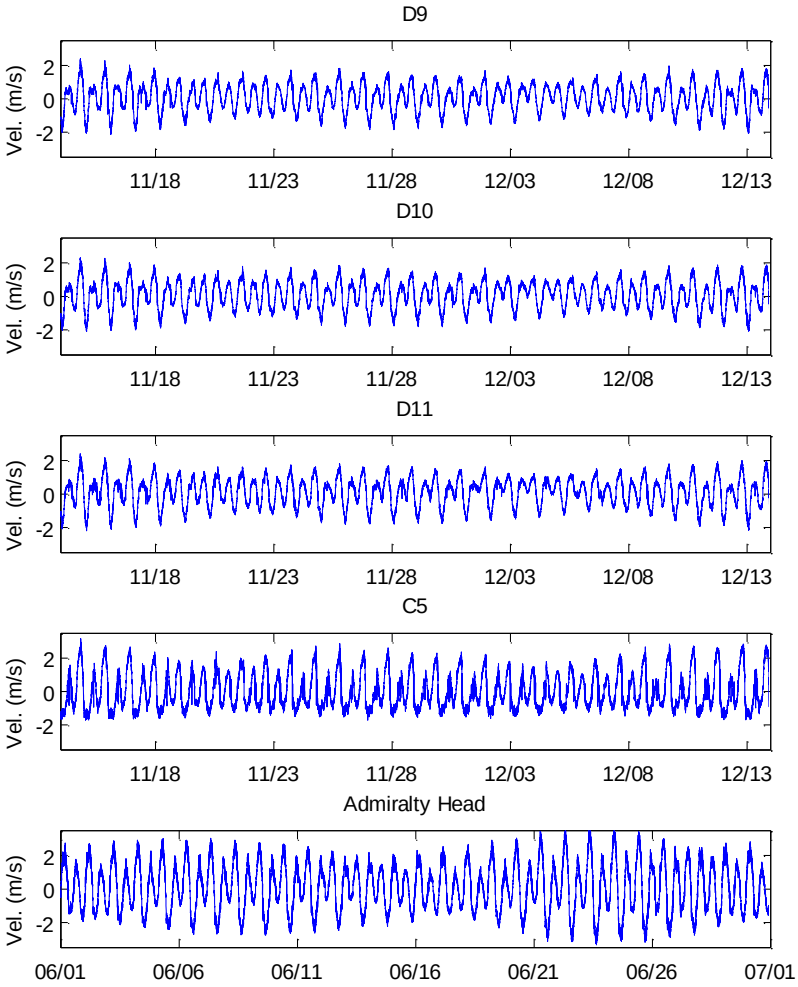

Figure 14. One month timeseries of the five test sites. Ebb is shown as positive velocity and flood as negative.

Velocity Parameters

Mean Velocity

Significance

The simplest possible metric, this can describe whether a site is of any preliminary interest for TISEC (tidal in-stream energy conversion).

Methodology

Velocity magnitudes for every ensemble at hub height are averaged during periods of ebb and flood and using all ensembles, including those at slack. Note that the velocity magnitude refers only to the horizontal components, and does not include the component in the vertical direction.

Results

Results are tabulated in the summary table on page 48. Based solely on this simple metric, the C5 site looks like the most promising of the Marrowstone sites with a mean speed of 0.95m/s, while Admiralty Inlet has the highest overall, with a mean speed of 1.26m/s.

Maximum Sustained Velocity

Significance

Maximum sustained velocity is a measure of the highest velocity "sustained" for a period of 5 minutes or more. This is important for preliminary site evaluation as well as turbine design considerations. This is similar to the metric proposed by EMEC, although the maximum velocity must be sustained for 10 minutes to meet their criteria [5].

Methodology

Ebb and flood hub height velocities are averaged in 5 minute windows. From these, the 5 minute window with the highest mean velocity is found. Note that

while higher instantaneous velocities occur elsewhere in the data, it is not "sustained" for any period of time and is of less relevance.

Results

Results are tabulated in the summary table on page 48. Again, the C5 site looks most promising of the Marrowstone sites, with a maximum sustained velocity of 2.9m/s. Admiralty again has the overall highest at 3.25m/s.

Velocity and Power Histograms

Significance

Velocity and power histograms provide a simple way to visualize the available resource at a site. The histograms indicate what percentage of the tidal cycle is useful for power generation. This metric is similar to the velocity distribution metric proposed by EMEC and described on page 7.

Methodology

The MATLAB routine for creating histograms is used. Results for each histogram bin are reported as a percent occurrence. Power density is computed as:

$$P = \frac{1}{2}\rho\langle v^3\rangle \tag{2.1}$$

where ρ is the nominal density of seawater (1025 kg/m^3). Average power density is computed by finding the power using the hub height velocity from every ensemble, and then taking the average of that number. Note that this is not the same as taking the cube of the average velocity. As in the EMEC recommendations, 0.1 m/s bins are used [5].

Results

As shown in Figure 15, site C5 has a much higher occurrence of larger velocities than the D sites. This is even more apparent in the kinetic power density shown

in Figure 16, where the power at C5 is in excess of 6 kW/m^2 at times, whereas the D sites rarely exceed 3 kW/m^2. Admiralty Inlet is again the overall highest. Comparison of the Marrowstone sites demonstrates the intensification of small differences in velocity upon conversion to power.

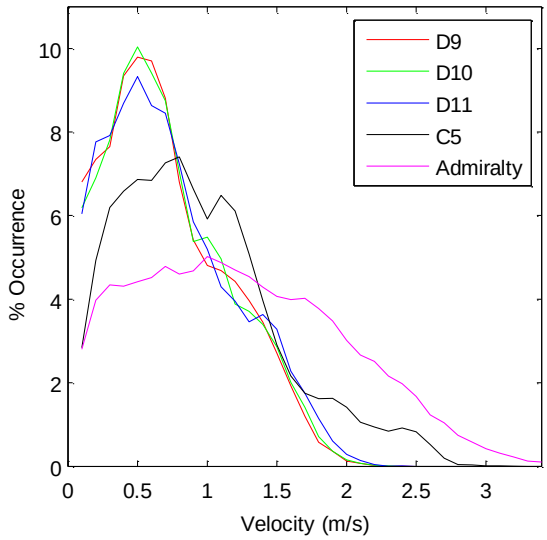

Figure 15. Velocity histograms as a percentage of total occurrences.

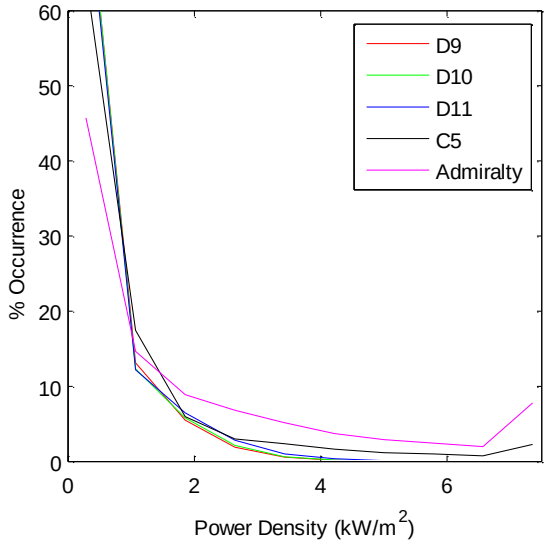

Figure 16. Kinetic power density histograms. Note that the increase in power density at the right hand end of the x axis indicates that power in excess of 6 kW/m^2 is generated at times.

Eddy intensity

Significance

Eddy intensity *(I)* is a quantification of the ratio of mesoscale velocity fluctuations to the background velocity, shown in Figure 17. These velocity fluctuations are characterized as turbulent structures on many different length scales caused by bathymetry and flow conditions of the same scale. These structures advected past the point of observation by the mean flow and are thus not expected to be useful for power generation [17].

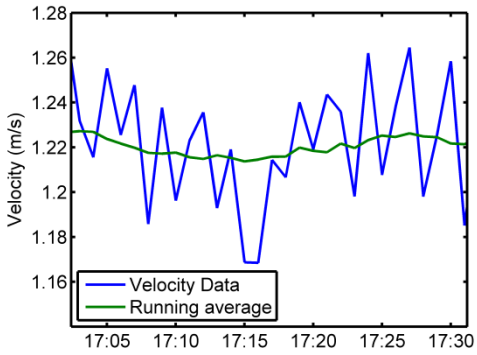

Figure 17. Velocity data (blue) and 15 minute running average (green). The difference between the two is the velocity anomaly *v'*.

Methodology

Eddy intensity is assessed using the following formula [18]:

$$I = \left\langle \frac{v'}{\bar{v}} \right\rangle - \left\langle \frac{n}{\bar{v}} \right\rangle \tag{2.2}$$

Where I is the eddy intensity (expressed as a ratio), v' is the velocity anomaly, $\bar{v}$ is a 15 minute centered difference velocity average, and n is the intrinsic noise in the ADCP measurement (depends on the working frequency, bin size, and pings per ensemble), which will bias eddy intensity measurements high [11]. The noise for these particular measurements is 1.1 cm/s. Note that the angle brackets represent a mean over the entire data set. All quantities are computed at the bin closest to the assumed hub height. The velocity anomaly $v' = v - \bar{v}$ represents the velocity with the temporal mean removed, and is calculated every for every observation using the centered difference running average $\bar{v}$. The time scale for the running average is chosen as a compromise between including enough individual observations to obtain a meaningful velocity anomaly and having a short enough window that the tide has not changed significantly (i.e., quasi-stationarity). This quantity is then averaged to create a single metric (the eddy intensity, I), for the site.

Results

Average eddy intensities are tabulated in the summary table on page 48. As expected, C5 has an eddy intensity slightly higher than the D sites. This is to be expected, as the Marrowstone headland likely generates eddies which are advected past the C5 site by the ebb currents [28]. Similarly high intensities on the flood tide are likely due to the weak mean velocities in the denominator of the metric, which result in a relatively high eddy intensity ratio. The Admiralty site also has higher eddy intensity on the ebb, likely due to the acceleration around Admiralty Inlet, as shown in Figure 38 on page 59.

Rate of Turbulent Kinetic Energy Dissipation

Significance

The rate of dissipation of turbulent kinetic energy (TKE) is a measure of how fast energy contained in turbulent motion is actually dissipated as heat and sound at a molecular (micro-scale) level. This is expressed in W/m^3, and is the rate of energy dissipation per unit volume (i.e., a true loss of energy from the flow, as opposed to advection of energy by the flow). This quantity does not describe the large-scale turbulent features quantified in the aforementioned eddy intensity metric, but only the actual dissipation occurring at a micro-scale. Thus, the resulting values for TKE dissipation rates are quite small, and probably of negligible concern for device performance. However, the TKE dissipation rate does provide a useful tool for comparing sites.

Methodology

The structure function method described by Wiles et al. [19] is used to compute the rate of TKE dissipation. The basic premise lies in using the turbulent component of the velocity data (velocity with the temporal mean removed, as in the section on eddy intensity) to determine the presence and behavior of eddies at

each specific point in time and space (in the z direction, since the ADCPs are stationary and uplooking).

The calculation begins by setting up the 2-dimensional structure function:

$$D(z,r) = \overline{(v'(z) - (v'(z+r))}^2 \tag{2.3}$$

D(z,r) is the mean-squared velocity fluctuation between two points separated by a distance *r*, as shown in Figure 18. Velocity fluctuations on the scale of *r* are largely due to turbulent structures of the same length and corresponding velocity scales. The value of *r* chosen must be smaller than the largest eddies – for the test cases presented here, a conservative value of 5 meters is used.

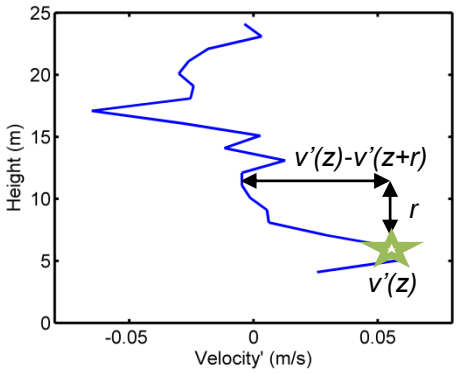

Figure 18. Profile of velocity with the mean removed v'(z) as a function of height. *D(z,r)* is the difference between *v'(z)* values separated by a distance *r*.

As described in the section on eddy intensity, v' represents the velocity anomaly, or the velocity with the running average removed. Using the Kolmogorov cascade theory, these characteristic scales are then used to determine the rate of TKE dissipation, expressed as ϵ, when fitted to a function of $r^{2/3}$:

$$D(z,r) = N + (C_v \epsilon^{2/3}) r^{2/3} \tag{2.4}$$

where N is an offset that represents uncertainty due to noise, and C_v is a constant, which in atmospheric studies is approximately 2.1 [29]. The length-scale

parameter r is from the previous equation. A sample of fitting to $r^{2/3}$ is shown in Figure 19 for values of the function at hub height. A successful $r^{2/3}$ fit validates the Kolmogorov cascade assumption. As expected, the velocity difference from a point will grow as the distance from that point becomes larger. Since C_v is a constant ϵ is the only independent variable, and therefore lines with higher slope have greater rates of TKE dissipation.

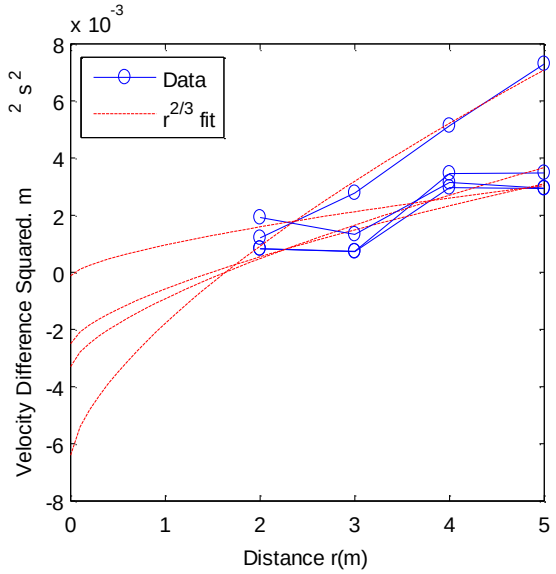

Figure 19. Velocity difference squared as a function of distance from the reference point (at hub height). Lines with greater slope represent higher dissipation estimates. Note that all fits shown in this graph are from hub height, and similar plots could be generated for all bins.

Results

A sample 24-hour result from site D9 is shown in Figure 20. This is typical of the entire deployment, and sub-set is shown simply for display purposes. As expected, the rate of TKE is greatest in the boundary layer near the seafloor, and is also generally greatest when the tides are strongest. Some anomalies are present during slack water, but this is to be expected, as a strong ebb/flood tidal shift is likely to cause dissipation. Averaged results for the entire deployment are shown in the summary table on page 48. C5 has a rate of TKE dissipation an order of magnitude larger than the D sites, which suggests a more turbulent environment,

and is consistent with the eddy intensity metric. Again, it is the relative comparison of ε between sites that is useful for tidal power evaluation, as opposed to the absolute ε value.

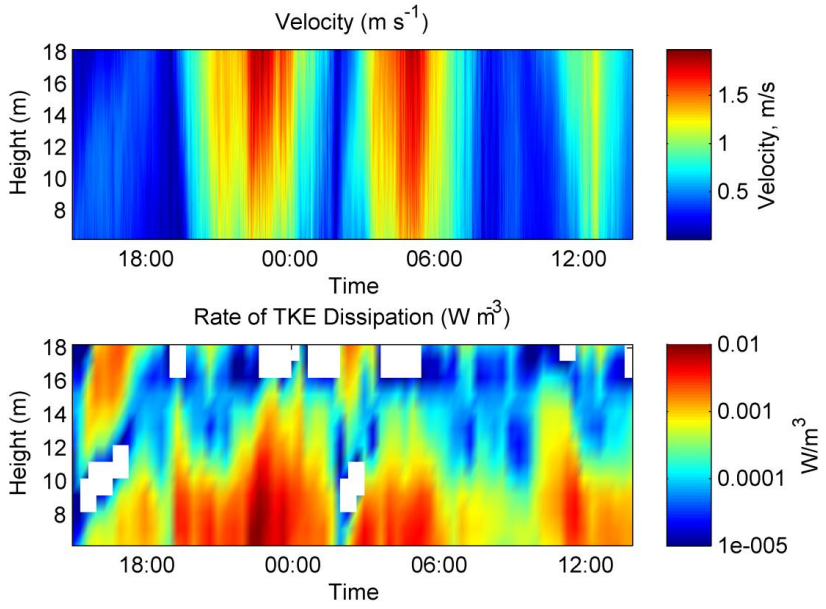

Figure 20. A 24-hour sample of velocity (top panel) and corresponding TKE dissipation rates at site D9.

Vertical Shear

Significance

The shear forces exerted by strong (1-3m/s) currents in a dense fluid such as water are significant from a mechanical design standpoint. The turbines must be designed to withstand not only the axial force exerted by the mean component of velocity, but also the shear force created by the velocity variations over the rotor span. These variations are due to the shape of the boundary layer as well as turbulent structures with length scales on the order of the size of the turbine. This makes them especially pertinent, as many turbines will likely be placed within the sea floor boundary layer. This metric is similar to that proposed by Lueck and Lu [15].

Methodology

The shear is calculated as a centered-difference using the bins below and above the hub height. Ebb and flood regimes are considered separately. The average shear is expressed as a scalar magnitude:

$$\frac{d|v|}{dz} = \frac{|v_{hh-1} - v_{hh+1}|}{\Delta z} \tag{2.5}$$

where the subscript "*hh*" denotes the bin closest to hub height. Note that while only the velocity magnitude is considered, the flow direction of each velocity component should be roughly similar. If the flows were markedly different in direction, this method would result in underpredictions, as velocities pointed in exactly opposite directions with equal magnitudes would show zero shear. However, cases where flow direction is very different likely occur around slack water when the tidal direction is shifting, and these profiles have already been eliminated using the 0.5m/s threshold.

Results

Average vertical shears are tabulated in the summary table on page 48. All sites have roughly the same shear on ebb tides, whereas on the flood the D sites are lower and the C5 site is higher. This is likely a function of the shape of the boundary layer, discussed on page 40. For practical application, these values can be multiplied by the rotor diameter to estimate the change in velocity from the bottom to the top of the rotor sweep. Note that this input condition may be changed by the presence of a turbine, which may normalize the upstream flow.

Asymmetry of Ebb/Flood Power and Velocity Magnitude

Significance

As exemplified by site C5 in Figure 22, an asymmetry in the velocity pattern can cause strong power generation on one side of the tidal cycle and weak generation on the other. This has implications for the total power produced, as well as the

usefulness of the power, as producing lots of power twice a day (i.e., only on one stage of the tide) is generally not as useful as producing four times a day. Recent research has shown TISEC devices may also affect sediment transport where large velocity asymmetries exist [30].

Methodology

The power and velocity asymmetries are computed as a simple ratio of P_{ebb}/P_{flood} and v_{ebb}/v_{flood}, respectively, where P and v represent the mean power density and velocity magnitudes.

Results

The D sites are all roughly equal in power availability on ebb and flood tides. The C5 site, in contrast, has 50% more ebb velocity and almost four times the power availability on the ebb tide. Results are tabulated in the summary table on page 48.

Directionality

Principal Axis Decomposition

Significance

Characterizing the principal axes of the tides is important for several reasons. It is a rigorous method of determining where ebb and flood regimes begin and end, which can be somewhat difficult to determine because of the two-dimensional nature of tidal currents. Treating ebb and flood regimes separately is important because each regime may have very different characteristics, and if treated together much of this information is lost. Almost all metrics treated in this document are based on the ebb-flood separation, and as shown in the summary table on page 48, it is often important to present the ebb and flood values for metrics as well as a weighted average.

Methodology

The principal axis decomposition is described here is based on code described in John Boone's book *Secrets of the Tide* [13]. This process essentially defines a new coordinate system where the principal axis (the x axis in this case) passes through the mean value and minimizes the sum-squared error of the data set. Formally, the new coordinate system is defined such that the greatest variance is described by the first principal component. To determine the principal axes, data is inputted as a two column matrix of north and east components. Calculations are all made at the assumed hub height. Velocities below 0.5 m/s are discarded. The mean of each component is found, and a matrix $\mathbf{X^T}$ is defined as the raw data with the mean removed. The principal axis transformation is given as:

$$\mathbf{Y^T} = \mathbf{X^T W} \tag{2.6}$$

where the vector $\mathbf{W}$ contains the eigenvalue which indicates the portion of the variance correlated with that eigenvector. Since $\mathbf{X^T}$ is a 2 column matrix, there will be two eigenvectors describing the 2D orthogonal axis components [31]. In the transformed coordinate system for these specific datasets, all ebb values have x values less than zero and all flood data greater than zero, as shown in Figure 21.

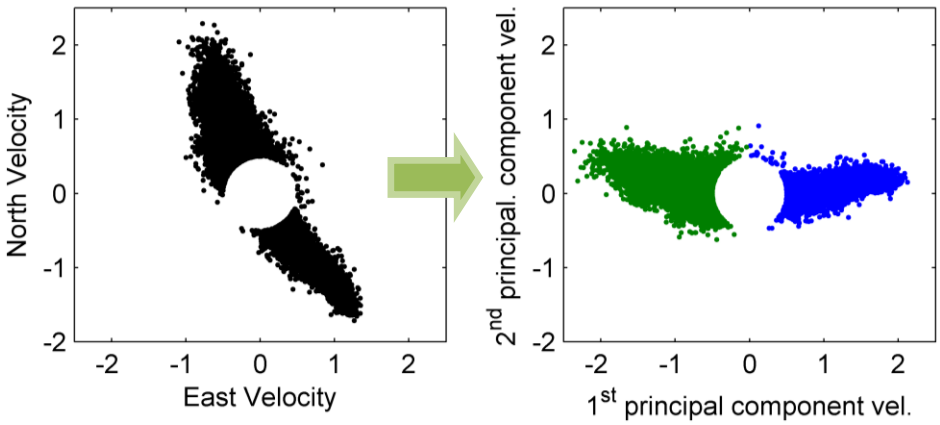

Figure 21. Transformation of raw velocity data from the D9 site (left) into data aligned on first principal axis (right) and categorized into ebb (green) and flood (blue) based on the criteria of x values being above or below zero.

Results

The principal axes at each of the four sites are shown in Table 3. Note that the "principal axis" encompasses both ebb and flood tides, and is therefore different than the mean angle values presented for ebb and flood tides in Figure 22.

Table 3. Principal Axes as calculated for all data, degrees from true north.

Site	D9	D10	D11	C5	Admiralty Inlet
Principal Axis (Degrees CW from N)	148	146	150	137	131

Directional Deviation and Asymmetry

Significance

Turbine models designed for bi-directional tides may not have sufficient yaw ability for asymmetrical ebb and flood conditions, and may not be able to efficiently extract energy from these off-axis currents [27]. Asymmetry is a measure of the bi-directionality of the ebb and flood flows. Deviation is a measure of the amount of directional deviation within the ebb and flood regimes. Large asymmetry or a large deviation in one regime could also lead to strong power generation on one half of the tidal cycle, and very little generation on the other. Furthermore, asymmetrical or deviant currents can indicate complex geometry in the region, which could increase the variability of tides and create a need for more precise and therefore more costly "micrositing" measures [15]. This could also potentially create future complications for placing multiple turbines at a site. This metric is similar to that proposed by Lueck and Lu [15] and shown in Figure 10 on page 19.

Methodology

Asymmetry is computed as the difference between ebb and flood angles. The direction is not particularly meaningful, so an absolute value is used:

$$Asymmetry = \left|\theta_{ebb} - \theta_{flood} - 180\right| \tag{2.7}$$

Using this formula, a perfectly bi-directional tide would have an asymmetry of zero degrees. Note that since this metric relies on direction, it was important to make sure that no points "wrapped around" from 360 degrees back to zero, especially important with the C5 ebb regime shown in Figure 22, where a large portion of the data straddles that area. To resolve this, all data in the ebb regime with angle less than principal axis+90 (those points that did "wrap around") had 360 degrees added to their angles. Since the principal axis is defined as the value in the first two quadrants (less than 180 degrees), the data are then within the ranges:

$$\begin{aligned} Flood &= PrincipalAxis \pm 90 \\ Ebb &= Principal\ Axis + 180 \pm 90 \end{aligned} \tag{2.8}$$

The resulting ranges of angles are shown in Table 3. Deviations are calculated as a simple standard deviation of the mean angles within each regime.

Results

As shown in Figure 22, site C5 is the least bi-directional site (i.e., largest asymmetry), and also has the largest standard deviation on both flood and ebb. Note that D9 was not included because of its similarity to the other D sites. C5 has the largest velocity magnitudes of any site, although only on the ebb tide. Asymmetries are tabulated in the summary table on page 48. Note that the angles presented here are different than the principal axes shown in Table 3, which encompass both ebb and flood tides.

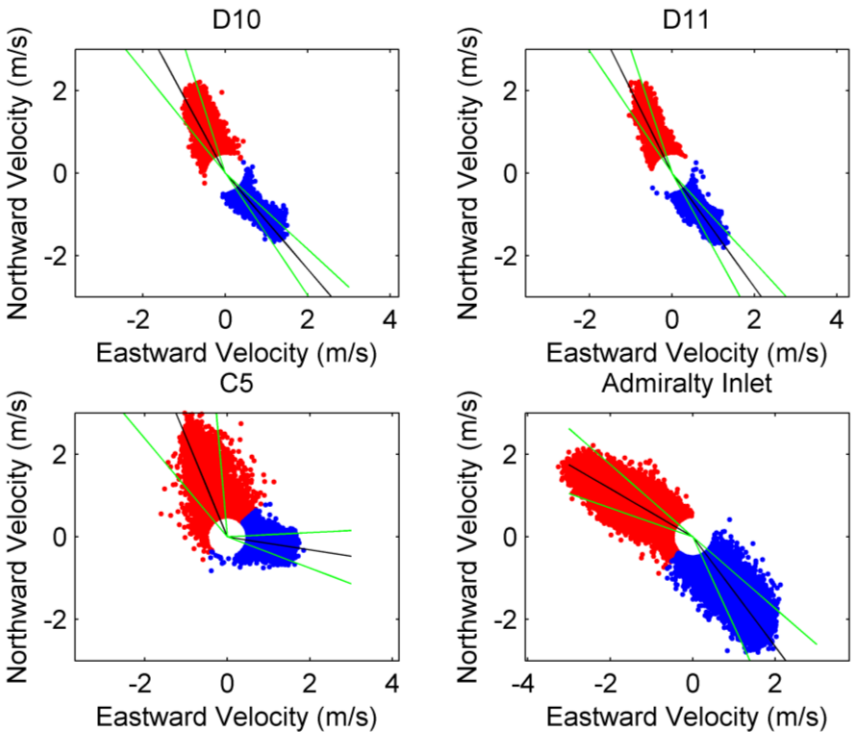

	D9	D10	D11	C5	Admiralty Inlet
Ebb	-30±12°	-28±10°	-26±8°	-23±17°	-60±11°
Flood	144±7°	139±7°	144±7°	99±12°	143±12°

Figure 22. Mean axes and standard deviations of ebb (red) and flood (blue) tides at hub height. Angles of mean axes and corresponding standard deviations are given in degrees CW from magnetic north. Note that D9 is not included because of its similarity to the other D sites.

Direction as a Function of Time

Significance

Similar to the method proposed by Lueck and Lu [15] shown in the upper panel of Figure 11 on page 19, this metric shows the flow direction at hub height as a function of time. If flow changes direction significantly within the ebb or flood, devices that do not yaw will experience decreased flux and reduced power input [27]. Additionally, devices that do have the ability to yaw may still not be able to respond if flow direction change extremely rapidly.

Methodology

Tides are again separated into ebb, flood and slack regimes using a principal axis decomposition. Dataset lengths are preserved so that ebb and flood data correspond to the correct timestamp.

Results

Direction at hub height for a sample 3 day period is shown in Figure 23. All sites tend to spike at the beginning and end of each regime, which is consistent with the results found by Lueck and Lu in Figure 11. All Marrowstone sites tend to rotate slowly through a shift of approximately 15-30 degrees, which could potentially affect the flux to devices without yaw capabilities. The C5 site is again the most erratic of the Marrowstone sites, with significant fluctuations occurring especially on the ebb. Note that although the "slack" points cover the entire directional range, these points are not considered ebb or flood because their magnitude does not exceed the 0.5m/s threshold. Restated, the magnitudes of the minor axes of the Marrowstone sites do not exceed the 0.5 m/s threshold until the direction of the flow has almost completely reversed. The Admiralty site, however, has points exceeding the 0.5m/s threshold at almost all angles, indicating the tidal ellipse will be "wider" than the Marrowstone sites (it will also be longer due to higher velocities at peak flood and ebb).

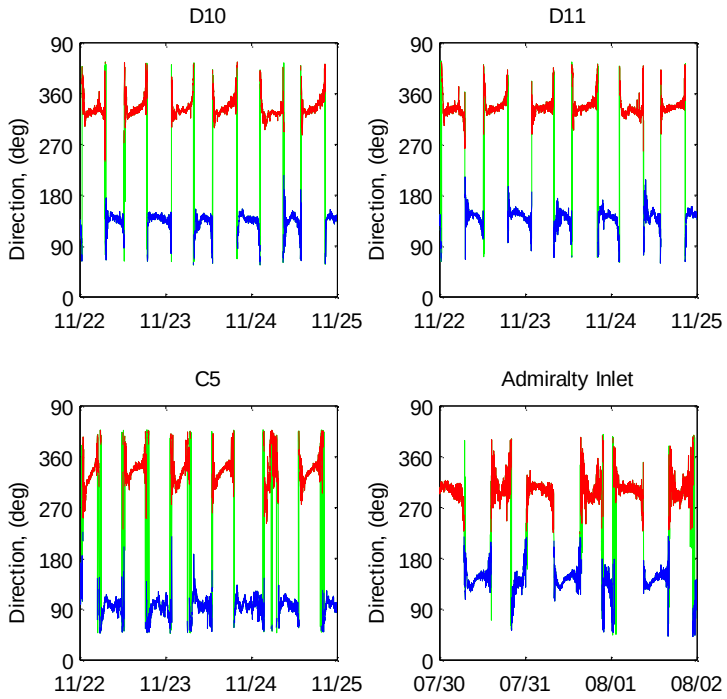

Figure 23. Direction at hub height as a function of time for an arbitrary three day sample, where blue indicates flood, red indicates ebb, and green is slackwater. Note that at the Marrowstone sites, although slack extends well into the ebb and flood regimes in terms of direction, these points are still less than 0.5m/s in magnitude and are therefore still considered slack. D9 is not included because of its similarity to the other D sites.

Vertical Profile

Boundary Layer Power Law Approximation

Significance

Tidal currents are generally maximal near the surface and diminished near the seabed. Understanding the reduction in velocity within the bottom boundary layer is essential for designing turbine foundations and determining a desirable hub-height. It has been suggested by previous studies [24] that the boundary-layer behavior of a fluid is best approximated by a power law of the form:

$$V(z) = V_0 \left(\frac{z}{d}\right)^{\frac{1}{\alpha}} \tag{2.9}$$

where V_o is the surface velocity, d is the depth of the fluid, $V(z)$ and z are the velocity as a function of depth and depth of the water of fluid, and α is the empirical constant, nominally 7 or 10 [24], [5]. The ability to model data with such a simple approximation is valuable for making generalizations based on sources of limited data, such as NOAA surface velocity predictions. These predictions can be extrapolated downwards to predict the velocities at the hub heights, possibly saving time and money in resource evaluation. In order to test the validity of these arguments, power law approximations are fitted to the stationary ADCP data to test whether these generalizations are valid.

Methodology

Instead of fitting a specified exponent such as $1/7^{th}$ to the data, this parameter is left as the dependent variable and is optimized through a least-squares fitting using the FIT toolbox in MATLAB. The fitting is performed for 15 minute average velocity profiles with all bins at hub height above 0.5 m/s. Fits with large residuals (R^2<0.5) are excluded. Note that most profiles with poor fits occur near slack where flow has reversed in part of the water column and are not of practical importance for resource assessment or device performance evaluation. Velocity profiles are characterized for ebb and flood tides, as well as in aggregate.

Results

For the Marrowstone case studies, an exponent between $1/4^{th}$ and $1/6^{th}$ is a more accurate representation than the $1/7^{th}$ generally assumed. Ebb tides tend to have exponents closer to the $1/4^{th}$, whereas flood tides tend to be closer to the $1/7^{th}$ law with the exception of C5, with an exponent of $1/3^{rd}$. The exponents closer to unity effectively create larger boundary layers by representing a slower decay in velocity from the surface value. As expected, the exponents correlate to the amount of vertical shear, as larger boundary layers will result in a greater velocity differential at hub height. Vertical shear is highest at C5 on the flood, when the $1/3^{rd}$ boundary layer is present. Shear is lowest at sites D9 and D10 on the flood,

when the steepest boundary layer (1/6.7) is present. It should be noted that the Marrowstone Island sites are very shallow when compared to other potential TISEC sites. Flow at the surface is still somewhat affected by boundary drag, meaning that a device may need to be placed higher in the water column to avoid adverse velocity and shear effects. This is much different than the profile of the much deeper Admiralty Inlet site, which is in agreement with the $1/10^{th}$ power laws found in previous literature shown in Figure 9 on page 18 [4].

At the Marrowstone sites, 80-90% of the data above 0.5m/s is well-described power law (i.e., the power law explains the observation). This number is closer to 70% at the Admiralty site. However, a power law exponent averaged across all profiles must be viewed with caution. As shown in Figure 24, this fit attempts to describe a wide range of data, whose behavior cannot be entirely accurately modeled with any single formula. It is likely that profiles nearer to the peak tide have a different curve than the average profile. Using other criteria for data exclusion will also change the shape of the profile, such as excluding all profiles with hub height speeds under 0.5m/s, or simply excluding all points under 0.5m/s. Again, this boundary layer approximation is intended for extrapolating data to hub height from existing predictions or 2D model data, which will have specific surface or depth-averaged velocities with which to fit the power law profile. The purpose of this analysis was solely to determine the correct power law exponent for use in these predictions, and not to attempt to describe the activity at the site in terms of a single formula.

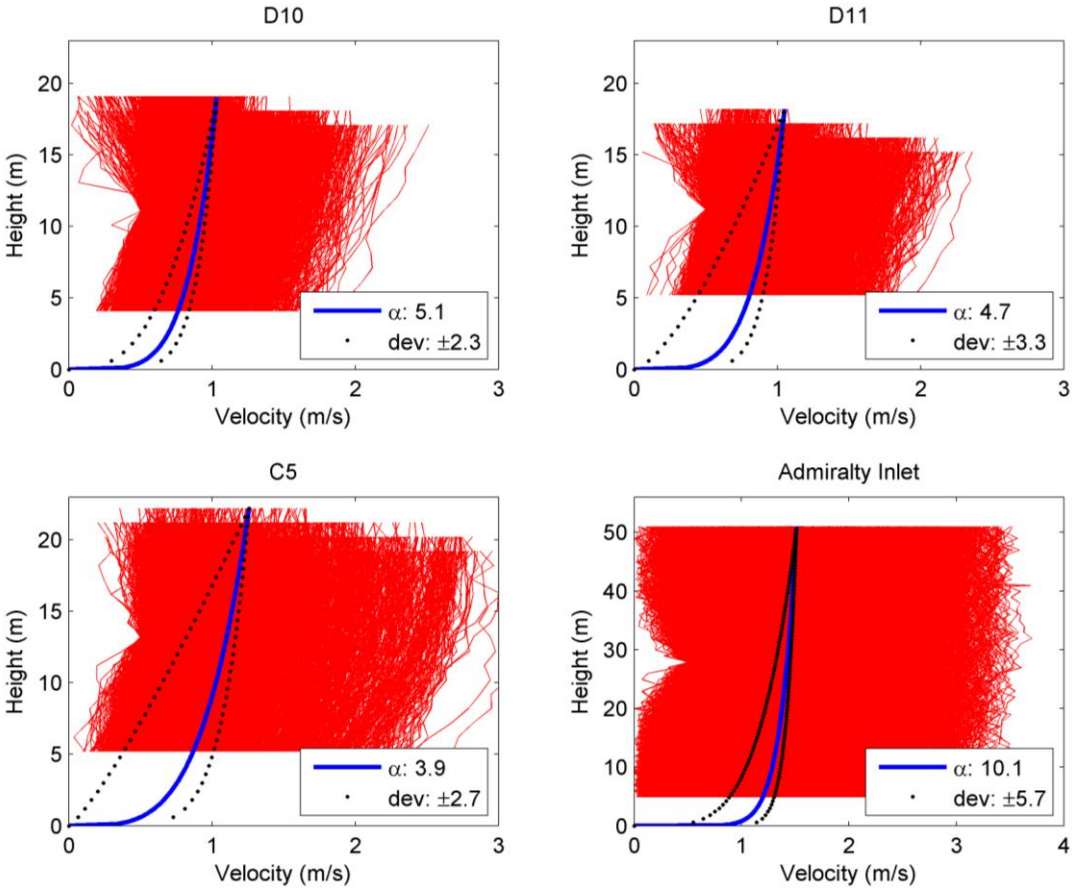

Figure 24. ADCP data and best-fit power law exponents. The black dots represent one standard deviation in the value of α using the fitted power law. Power laws are plotted using mean surface velocity, although for fitting purposes all profiles were fitted individually.

Vertical Profile Directionality

Significance

This metric shows the averaged direction for the ebb and flood regimes as a function of height. Large direction differences over the rotor span could result in unwanted shear forces and could reduce the amount of available power if much of the fluid flux is off-axis. Comparing standard deviations at sites is useful for determining flow variability within the water column and between sites. This metric is similar to that proposed by Lueck and Lu [15] and shown in plots (a) and (b) in Figure 11 on page 19.

Methodology

Flows are separated into ebb and flood profiles based on the velocity direction at hub height using the principal axis decomposition described previously. The standard deviation is calculated at each height using the profiles within that regime. Values are truncated 2m below the reported averaged surface height, as wind and wave activity towards the surface introduce noise into the data and create extremely high deviations.

Results

As shown in Figure 25, mean directionality as a function of height is roughly equivalent at all four sites, with no large variations occurring at any height. Variability as expressed as standard deviation is much higher on ebb tides (shown in blue), with the C5 site having especially high values throughout the water column. Although profiles are truncated 4m below the surface, motion due to wind and waves still play a large role near the surface and create large deviations which occur in all profiles. The D11 site has another area of high deviation around 10m on the flood, which would likely be around the height a turbine would be positioned. Higher deviations in the D sites towards the bottom of the water column on ebb tides indicate that these flows could be more erratic and contain more turbulent activity within the boundary layer.

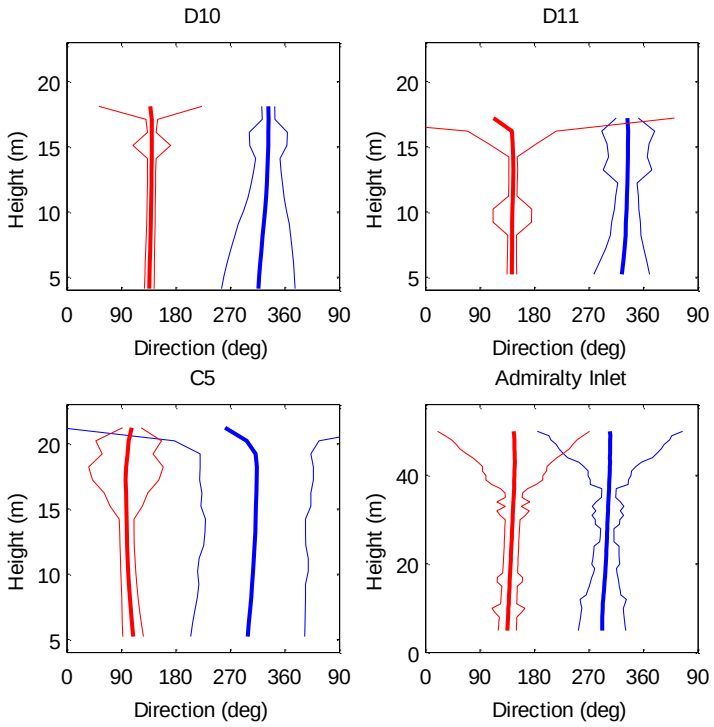

Figure 25. Averaged direction and standard deviations as a function of height for ebb (blue) and flood (red). Even with the top four bins below surface height removed, it can still be seen that directional variation is much higher at the top of the water column, presumably because of wind and wave effects. Note the height scale is different at Admiralty Inlet.

Corrections to NOAA Current Predictions

Significance

Comparing ADCP data to nearby NOAA current stations serves several purposes. As a first step, it is important to determine the quality of the NOAA predictions and assess whether it is an accurate representation of the current in the area. If the data does correlate, it could potentially be used in conjunction with the mobile data to create a "phase corrected" map of the area.

Methodology

Corrections to NOAA data are made as simple phase and magnitude offset. Adjustments to the parameters are made until the ADCP and NOAA velocity magnitudes are best aligned. A more rigorous approach would be to correct every

tidal constituent for ebb and flood, but this is expected give noticeably better results only for longer datasets. For the Marrowstone case studies, the "D" sites are compared to the nodule point NOAA station. The C5 site is compared to the site 1.6 miles northeast of Marrowstone point. These stations are shown in Figure 26.

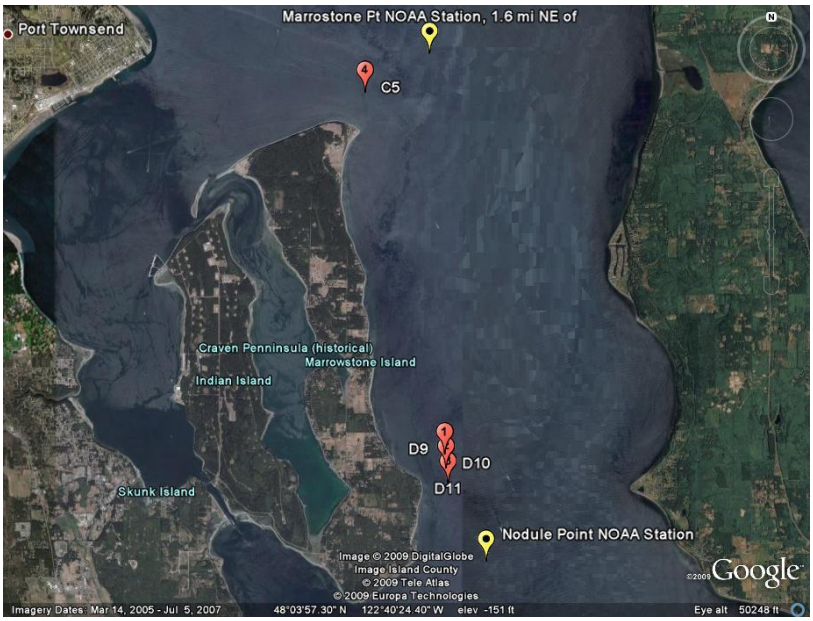

Figure 26. ADCP and NOAA station locations. Images © DigitalGlobe 2009, © TeleAtlas 2009

Results

A simple phase and magnitude offset seems to do a relatively good job of modeling data at the Marrowstone sites. Ebb tides are slightly underpredicted, and flood tides slightly overpredicted. As NOAA predictions are based on harmonic decomposition, it is likely that these effects are due to non-tidal causes such as local bathymetric influence [13]. It is likely that the contour of Marrowstone Island directly north of the D sites has an accelerating effect, contributing to the faster floods in that area.

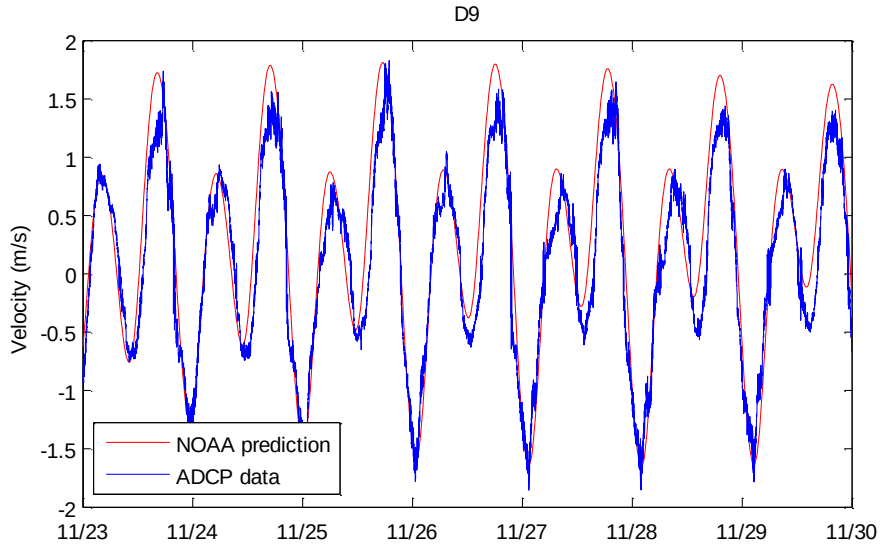

Figure 27. A sample of NOAA surface velocity data (in red) shifted by 1.7 hours to correspond to ADCP data at site D9 (in blue). Ebbs are shown as positive and floods as negative velocities.

Conclusions

A set of methodology is described to analyze stationary ADCP data for the purpose of tidal power site characterization. Using sites along the northern and eastern shores of Marrowstone Island as case studies, it is shown that average power density is not sufficient to describe the suitability of a site. Although Marrowstone C5 has substantial power density, the site is asymmetric (ebb dominated), turbulent, and directionally variable compared with the more laminar sites of D9, D10, and D11. The metrics presented in this section are intended to be used in the TISEC selection process, and are designed to be device neutral. Further analysis will require specific information about the nature of the TISEC device with regard to its height, diameter, yaw capacity, response time and failure modes, among others [27]. It is likely once a device is selected additional parameters not discussed in this report will become relevant for final site selection.

Summary of Results (Table 4)

Summary Statistics[a]					
	Marrowstone				Admiralty
Site	D9	D10	D11	C5	Inlet
Velocity					
Mean speed (m/s)	0.72	0.73	0.75	0.95	1.26
Max sustained[b] speed (m/s)	2.12	2.12	2.19	2.24	3.25
Eddy intensity (%)	2.9%	3.1%	2.8%	5.2%	5.4%
Ebb/flood asymmetry	0.97	0.98	0.93	1.47	1.06
Vertical shear (m/s per m)	0.023	0.024	0.027	0.033	0.031
Turbulent dissipation $(W/m^2)10^{-5}$	1.9	2.2	2.6	7.5	10.8
Power					
Mean power density (kW/m^2)	0.42	0.43	0.48	0.98	2.10
Ebb/flood asymmetry	0.9	0.9	0.8	3.9	1.20
Direction					
Principal axis[c] (deg CW from N)	148	146	150	137	131
Standard deviation (deg)	10	9	7	14	12
Ebb/flood asymmetry (deg)	6	12	9	58	23
Vertical Profile					
Assumed hub height[d]	12.6	11.5	10.7	12.7	27.8
Mean depth (m)	25	23	21	25	56
Power law exponent $1/(\alpha)$[e]	5.2	5.1	4.7	3.9	10.1
Standard deviation of α	2.5	2.3	3.3	2.7	5.7
% of profiles fit	81%	91%	94%	96%	72%
NOAA Corrections					
Phase lead/lag (hours)	-1.7[f]	-1.7[f]	-1.7[f]	0.0[g]	-
Amp. correction to ADCP data	0.90	0.95	0.95	1.25	-
Sit					
Measurement duration (days)	33	33	33	33	75
Vertical resolution (m)	1	1	1	1	1
Sampling interval (min)	1	1	1	1	0.5
Data collected by		OARS			NNMREC

[a] Reported at middle of water column
[b] "Sustained" over a 15 minute window.
[c] Angles are reported from magnetic north. 180 degrees are subtracted from the ebb direction so that a meaningful average of ebb and flood directions can be computed.
[d] Assumed hub height is half of water depth.
[e] Assuming vertical profile is of the form $u(z) = u_0(z/z_0)^{1/\alpha}$.
[f] Corrected to Nodule Point NOAA station
[g] Corrected to NOAA station 1.6 mi NE of Marrowstone Point

Ebb Statistics[h]					
Site	Marrowstone				Admiralty Inlet
	D9	D10	D11	C5	
Velocity					
Mean speed (m/s)	0.95	0.95	0.97	1.41	1.50
Max sustained speed (m/s)	2.19	2.24	2.29	3.03	3.41
Eddy intensity (%)	2.9%	3.1%	2.9%	5.1%	6.2%
Vertical shear (m/s per m)	0.025	0.026	0.028	0.028	0.033
Direction					
Principal axis (deg CW from N)	-30	-28	-26	-23	-60
Standard deviation (deg)	12	10	8	17	11
Vertical Profile					
Power law exponent 1/(α)	4.4	4.5	4.4	5.5	11.3
Standard deviation of α	2.4	2.2	2.8	3.8	6.5
% of profiles fit	94%	98%	96%	94%	77%
Power					
Mean power density (kW/m^2)	0.61	0.63	0.68	2.20	2.78

Flood Statistics					
Site	Marrowstone				Admiralty Inlet
	D9	D10	D11	C5	
Velocity					
Mean speed (m/s)	0.98	0.98	1.04	0.96	1.41
Max sustained speed (m/s)	2.01	1.95	2.04	1.63	3.08
Eddy intensity (%)	2.8%	3.2%	2.7%	5.4%	4.5%
Vertical shear (m/s per m)	0.020	0.022	0.026	0.037	0.030
Direction					
Principal axis (deg CW from N)	144	139	144	99	143
Standard deviation (deg)	7	7	7	12	12
Vertical Profile					
Power law exponent 1/(α)	6.2	5.9	5.2	2.7	8.9
Standard deviation of α	2.7	2.4	4.0	1.8	4.9
% of profiles fit	82%	81%	90%	97%	65%
Power					
Mean power density (kW/m^2)	0.69	0.69	0.81	0.57	2.31

[h] Reported at middle of water column. All speeds greater than 0.5 m/s

Part III: Mobile Data Interpolation

Introduction

It is well known that the power input to a TISEC device scales with the cube of the current velocity, and therefore proper siting is critical to the success of an installation [4]. What is less clear at this point is the effect of "micrositing", or the analysis of turbine placement on the scale of 10s of meters at a given location. It has been recommended in previous studies that 3D modeling and multipoint velocity measurements be undertaken before turbines are deployed although in many cases TISEC devices are also constrained to a particular water depth and/or hub height, which limits the amount of freedom in their placement [27]. This report intends to address the effect of micrositing for the Marrowstone Island site by using mobile velocity data to determine the spatial variation in the kinetic resource. This data was collected by Evans-Hamilton and was originally used to determine the placement of the four stationary ADCPs, whose data were used in the previous section.

Methodology

The basis of this analysis is an interpolation of mobile data measurements made in linear transects running roughly perpendicular to bathymetry and flow (Figure 28). Mobile data measurements are taken from transects made by Evans-Hamilton intended for the selection of the four stationary ADCP locations as described on page 20. Data from the three "D" transects are used, as well as the neighboring D8 and D12 transects. Bathymetric data are taken from the NOAA National Geophysical Data Center's US Coastal Relief Model Grids, which have a resolution of 3 seconds [32]. However, for the purposes of finding intersecting points between the transects and the bathymetry data, this resolution is not sufficient so bathymetry is interpolated using the GRIDDATA routine in MATLAB. WGS2UTM is used to shift bathymetry from WGS latitude and longitudinal

coordinates to Universal Transverse Mercator (UTM) northing and easting coordinates, expressed in meters, which simplifies subsequent distance calculations. Note that this must occur after the interpolation, as MATLAB requires a regularly spaced grid for a GRIDDATA interpolation. Bathymetry data within a certain range (nominally 50 meters) of ADCP data is then found, and if multiple points meet the criteria, only the closest one is used. This is repeated for all transect points. Isobaths (lines of constant depth) which intersect multiple transects are flagged, as these form the basis of the interpolation. Velocities are then interpolated along the length of these isobaths between the known values at the transects and using the points from the interpolated bathymetry. This is accomplished by computing the along-isobath distance between transects and performing a spline interpolation with INTERP1 across all transects which creates a smooth transition between known values as shown in Figure 30. Using a linear or nearest fitting routine does not take advantage of the ability to interpolate across multiple transects, which allows for more realistic modeling of where points of inflection (velocity maxima and minima) will occur. For this study, data collected during the ebb tide is used, as it is of higher quality than the flood data due to technical problems during the collection process [26].

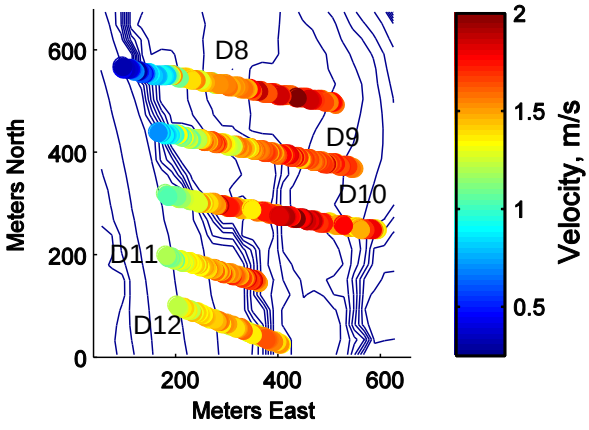

Figure 28. Mobile ADCP data collected roughly perpendicular to isobaths.

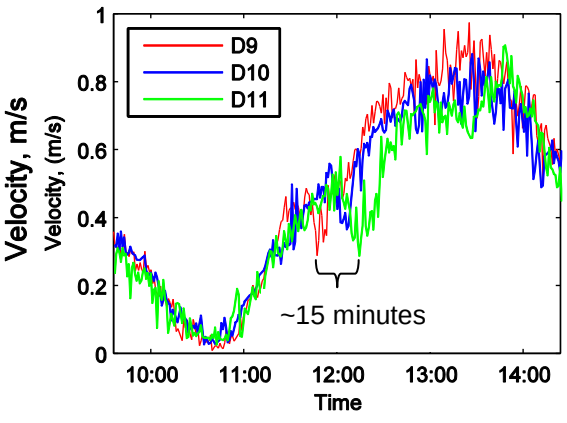

Figure 29. A sample of stationary ADCP data shows the small phase difference between transects.

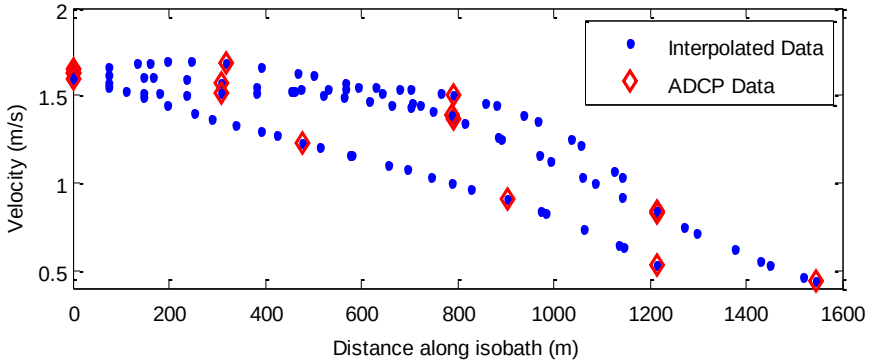

Figure 30. Spline interpolations performed between known velocity values from mobile ADCP transects (shown in red) along the lengths of isobaths. Note that the distance between transect data is not constant as isobaths are not straight and transects are not completely perpendicular.

The foremost assumption in making these calculations is that flow will tend to follow the bathymetry at a site. From a fluid mechanics standpoint, this is justified by the conservation of vorticity, which states that the angular momentum of any spinning body (such as an eddy being advected by the tides) is conserved [33]. Since a change in water depth will cause the relative vorticity of such a body to change, these features will tend to follow lines of constant depth so as to maintain their vorticity. This is a crude assumption, but of practical use when a full numerical model is not available.

Another assumption taken in making the interpolations is that the phase difference across transects is negligible. This is necessitated by a lack of co-temporal stationary ADCP data, which could be used to determine the peak ebb and flood and therefore adjust for phase differences as a function of position and time of data acquisitions. However, since the area surveyed in this case is relatively small (less than 1km in length) and the surveys were performed quickly (in about 35 minutes), these variations are neglected. Stationary ADCP data collected at the D9, D10 and D11 transects shows that the phase difference in the along channel direction is very small (Figure 29). A harmonic decomposition of

the tides shows that the two largest constituents, the M_2 and K_1, vary between sites by a maximum of only 3.4 and 7.3 minutes, respectively. It is important to keep in mind that all velocities used in this analysis are instantaneous and occur near peak ebb or flood, but are still only snapshots and do not necessarily represent the absolute maximum velocities.

Results

The basic interpolation map is shown in Figure 31 using an arbitrary 1 meter isobath interval. While this yields some useful information about the site, further analysis provides more useful metrics for the purpose of siting TISEC devices.

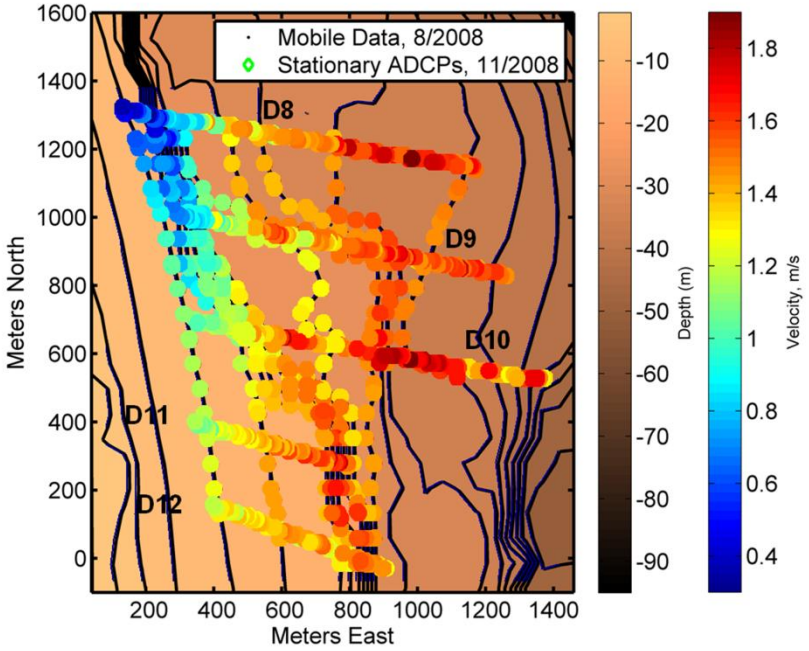

Figure 31. Velocities interpolated along isobaths using mobile ADCP data.

Percent Difference Along Transects

As mentioned previously, TISEC devices are often constrained to a maximum deployment depth for technical reasons and a minimum overhead clearance for shipping [34]. This may mean that in some cases adjustments to device location must be made roughly along a set of isobaths. This is especially relevant at

shallower locations, such as the Marrowstone sites. To this end, it is useful to know the change in velocity as a function of distance along the isobath in question. For the deployment at Marrowstone Island, a target deployment depth of 20-24 meters is assumed. Velocity data interpolated along these isobaths are averaged to find the change in velocity along the corridor most likely to be used for the TISEC deployment (Figure 33). It was found that velocities do not change dramatically in the along-isobath direction on the scale of 100s of meters, with a maximum change in peak velocity of only ~0.2 m/s per 100m. Additionally, it is likely that any differences are over-stated, as flow will not follow bathymetry as precisely as is assumed in this report, which will lead to more gradual velocity shifts and smaller differences.

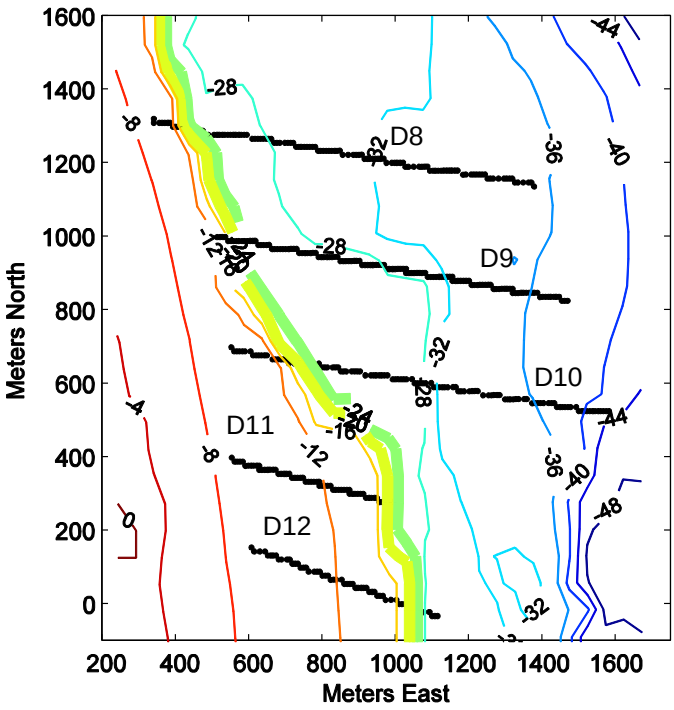

Figure 32. Bathymetry (m) at Marrowstone Island site. Contours at desired deployment depth range are highlighted.

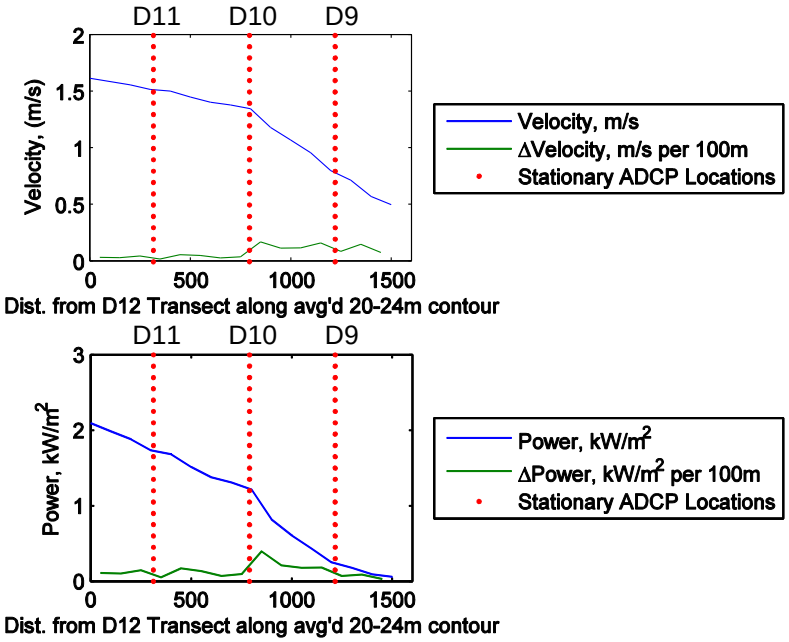

Figure 33. Changes in Velocity and Power as a function of distance along an averaged depth contour for 20-24m isobaths.

2-D Bathymetry-Interpolated Velocity Map

Another useful result for site analysis is a 2D "velocity map" of currents at a site, shown in Figure 34. This provides an easier way to visualize trends in currents than looking at raw data. The velocity map is made by performing an additional 2D interpolation of the transect data and the data interpolated along the isobaths using GRIDDATA. Note that in areas where no isobath interpolation exists the map has been cropped, as data interpolated between transects alone has little physical basis. For comparison, a velocity map interpolated using only data collected along transects is shown in Figure 35.

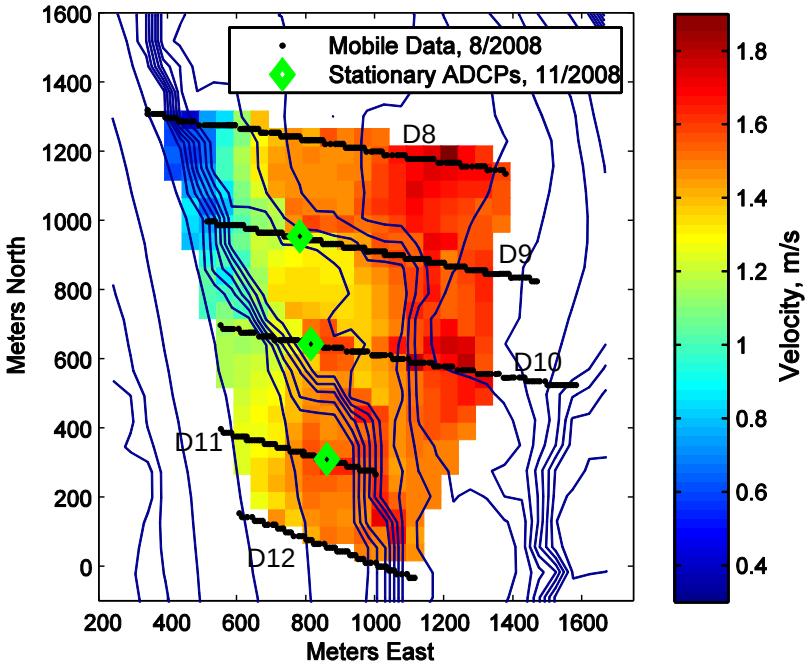

Figure 34. 2D "bathymetry-following" velocity map constructed from data interpolated along isobaths.

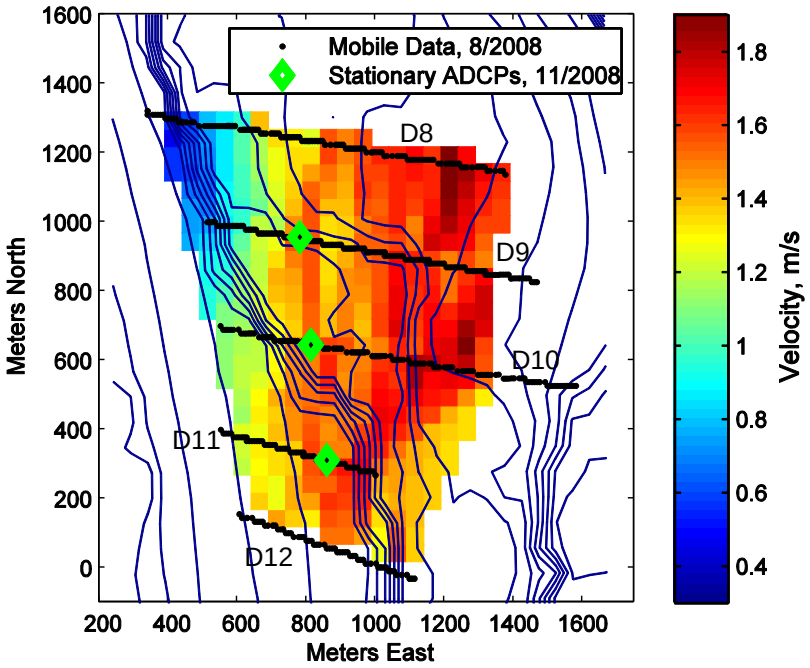

Figure 35. 2D velocity map interpolated using only transect data.

'Skill' Test

While it is easy to qualitatively compare the results of the bathymetric and interpolated methods, a more rigorous approach for quantifying the quality of the results is of more practical value. A 'skill' test for the two methods was devised in which one of the middle transects (D9 or D11) was removed so to compare the predicted values to the actual values from the ADCP data. The results are generally truncated for the interpolated method, as this relies on the isobath-transect intersections which did not occur along the entire length of the middle transects. Results show that in some cases, the interpolated method actually performs better than the bathymetric method, indicating that the assumption that flow follows bathymetry may not be valid under the flow and bathymetry conditions typical of TISEC sites (Figure 33). It should be noted that the predictive skill of both models is still relatively good, and is generally accurate to 0.1 m/s.

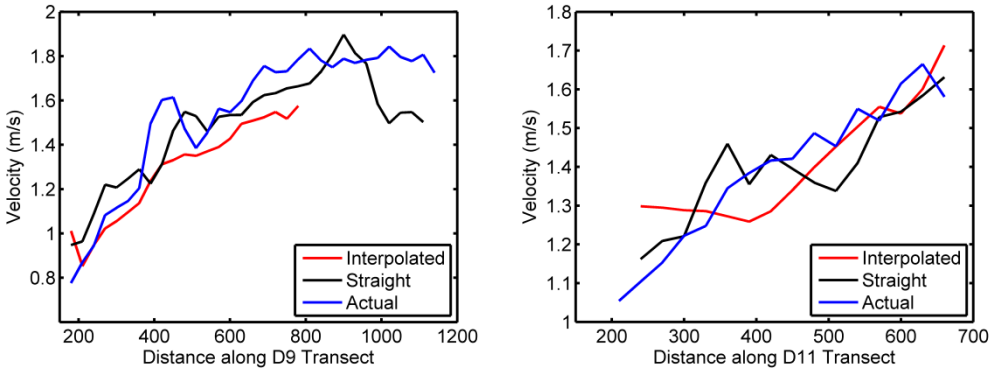

Figure 36. 'Skill' test of the bathymetric and interpolated 2D velocity mapping methodologies.

The 'quiver' plot in Figure 37 shows that even in areas with relatively simple bathymetry, flow does not closely follow bathymetry. While for many approximations in oceanography this difference is acceptable, the results of the skill test indicate that the bathymetry-following interpolation scheme requires higher correlation to produce significant gains over the normal interpolation scheme.

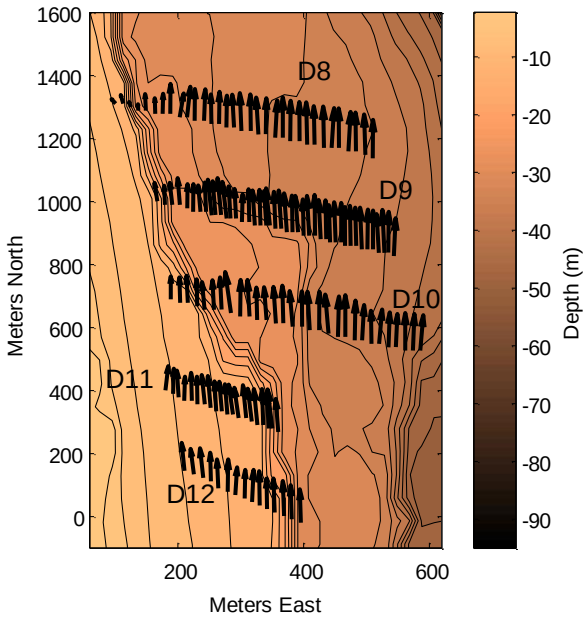

Figure 37. Quiver plot showing direction of velocities along mobile transects. Even in areas with relatively simple bathymetry, it can be seen that flow does not closely follow the contours, thereby decreasing the quality of the along-isobath interpolation.

Further error in the bathymetry-following method occurs when bathymetry has severe shifts or "doubles back" on itself, which requires corresponding shifts in projected flow. These shifts are most likely not non-physical, and in some cases provide contradictory results to the ADCP data. GRIDDATA averages these results, although a more rigorous approach would use only the ADCP data. Errors in the non-bathymetric interpolated method are caused by an entirely non-physical interpolation process, which in this case uses a primarily north-south route between the primarily east-west transects. This causes the non-physical artifacts such as "streaks" and sudden jumps in velocity.

Other Considerations

Note that these kinetic resource maps are based on ebb data. Flood data would likely produce a different map, based on local bathymetry and features such as headlands, which can create large scale eddies in one direction, as exemplified by the flow around Admiralty Head, shown in Figure 38 [7]. Unfortunately, flood

data for this site is more erratic due to technical problems during collection, and preliminary map iterations were of lower quality as those constructed using ebb data.

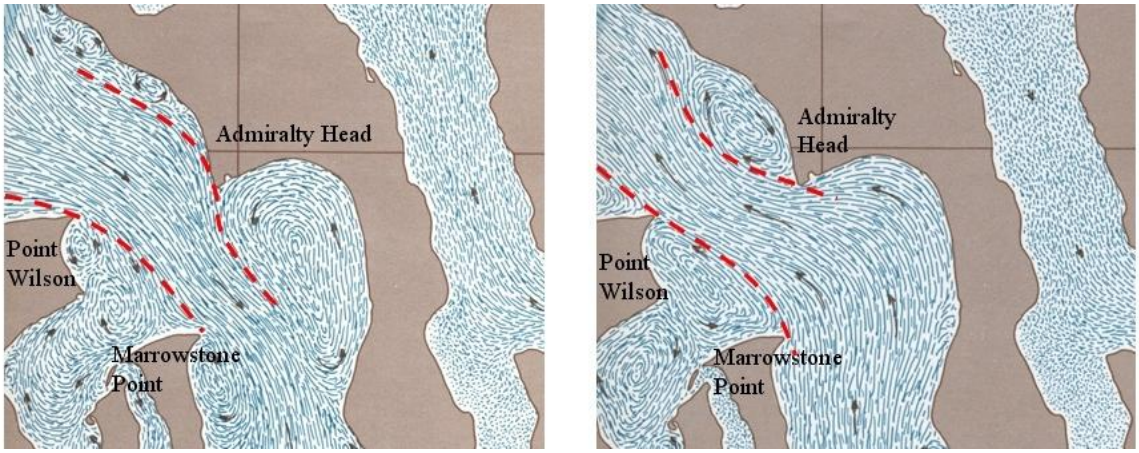

Figure 38. Flood (left) and Ebb (right) currents around Admiralty Head, exemplifying the possibility that flow will not follow bathymetry on both ebb and flood tides and may invalidate the assumptions made in the generation of the kinetic resource map [7].

Conclusions

Preliminary trials of the kinetic resource map have been relatively promising. However, these results may not apply to all sites, as results are highly dependent on local bathymetry and flow conditions. The assumption of flow following bathymetry will not be valid if the mean flow is not roughly perpendicular to isobaths. In sites with more complex bathymetry, flow will most likely not follow the contours of the seafloor closely and the assumption will break down.

Future iterations of this analysis might employ additional interpolation techniques, such as a "progressive vector diagram", where known velocity directions are extrapolated to neighboring transects, and so on. These extrapolated lines can then form the basis of a spline velocity interpolation similar to that used in the bathymetry-following scheme. This is designed to simulate a Lagrangian "particle following" model from Eulerian (fixed coordinate) data, and is commonplace in atmospheric and oceanic sciences [35]. This would provide a

reasonable substitute for bathymetric interpolation in areas where such an assumption is illogical or produces erratic results.

List of References

[1] The Associated Press. (2009, March) Navy to test tidal power in North Puget Sound. [Online]. http://www.oregonlive.com/environment/index.ssf/2009/03/navy_to_test_tidal_power_in_no.html

[2] Sam Reed. (2006) Initiative 937. [Online]. http://www.secstate.wa.gov/elections/initiatives/text/i937.pdf

[3] Black and Veatch, "PHASE II UK Tidal Stream Energy Resource Assessment," lsleworth, 2005.

[4] George Hagerman and Brian Polagye, "Methodology for Estimating Tidal Current Energy Resources and Power Production by Tidal In-Stream Energy Conversion (TISEC) Devices," in *EPRI North American Tidal In Stream Power Feasibility Demonstration Project*.: EPRI, 2006.

[5] Claire Legrand, "Assessment of Tidal Energy Resource," The European Marine Energy Center, London, 2009.

[6] N. R. Pettigrew, R. C. Beardsley, and J. D. Irish, "Field evaluations of a bottom mounted Acoustic Doppler Profiler and conventional current meter moorings," in *IEEE Third Working Conference on Current Measurement, January 22-24, 1986*, Airlie, 1986.

[7] Brian Polagye, Mirko Previsic, and Roger Bedard, "Tidal In-Stream Energy Conversion (TISEC): Survey and Characterization of SnoPUD Project Sites in the Puget Sound," in *EPRI North American Tidal In Stream Power Feasibility Demonstration Project*.: EPRI, 2007.

[8] Ian Bryden and G T Melville, "Choosing and evaluating sites for tidal current development," vol. 218, 2004.

[9] Burton Hamner, "Tacoma Narrows Tidal Power Feasibility Study," Seattle, 2007.

[10] E. Droniou and J. V. Norris, "Update on EMEC activities, resource description, and characterisation of wave-induced velocities in a tidal flow," in *7th European Wave and Tidal Energy Conference*, Porto, Portugal, 2007.

[11] "Acoustic Doppler Current Profiler Principles of Operation: A Practical Primer.," RDI Instruments, 1996.

[12] "Department of Defense World Geodetic Syetem 1984: Its Definition and Relationships with Local Geodetic Systems," The Department of Defense National Imagery and Mapping Agency, 2000.

[13] John D. Boon, *Secrets of the tide: tide and tidal current analysis and applications, storm surges and sea level trends*.: Horwood Publishing, 2004.

[14] Rich Pawlowicz, Bob Beardsley, and Steve Lentz, "Classical tidal harmonic analysis including error

estimates in MATLAB using T_Tide," vol. 28, 2002.

[15] Youyu Lu and Rolf G. Lueck, "Using a Broadband ADCP in a Tidal Channel. Part I: Mean Flow and Shear," *J. Atmospheric and Oceanic Tech.*, vol. 16, pp. 1556-1568, November 1999.

[16] Navy operational ocean circulation and tidal models, Basic Concepts in Physical Oceanography: Tides. [Online]. http://www.oc.nps.edu/nom/day1/partc.html

[17] Pijush Kundu and Ira Cohen, *Fluid Mechanics*. San Diego: Academic Press, 2002.

[18] Erik L. Petersen, Niels G. Mortensen, Lars Landberg, Jørgen Højstrup, and Helmut P. Frank, "Wind Power Meteorology," Risø National Laboratory, Roskilde, Denmark, 1997.

[19] Phillip J Wiles, Tom P Rippeth, John Simpson, and Peter J. Hendricks, "A novel technique for measuring the rate of turbulent dissipation in the marine environment," *Geophysical Research Letters*, vol. 33, no. L21608, November 2006.

[20] A. E. Gargett, "Velcro measurement of turbulence kinetic energy dissipation rate epsilon," *J. Atmos. Oceanic Technology*, vol. 16, no. 12, pp. 1973-1993, 1999.

[21] Youyu Lu and Rolf G. Lueck, "Using a Broadband ADCP in a Tidal Channel. Part II: Turbulence," *J. Atmospheric and Oceanic Tech.*, vol. 16, pp. 1568-1579, November 1999.

[22] O.B. Fringer. (2006) Source code for SUNTANS: Stanford Unstructured Nonhydrostatic Terrain-following Adaptive Navier-Stokes Simulator. [Online]. http://suntans.stanford.edu

[23] Kristen Thyng, "State of NNMREC Modeling," University of Washington NNMREC, Seattle, Presentation 2008.

[24] E.W. Peterson and J.P. Hennessey Jr., "On the use of power laws for estimates of wind power potential," *J. Appl. Meteorology*, vol. 17, pp. 390-394, 1978.

[25] "The Exploitation of Tidal and Marine Currents," Commission of European Communities Program JOULE II, EUR 16683 EN, No. JOU2-CT93-0355, 1996.

[26] Mary Ann Adonizio, Hannah Abend, Susana Crespo, and Dean Corren, "NPS - Stationary ADCP locations - Work under CDRL A009," Verdant Power, New York, Memorandum 2008.

[27] Roger Bedard, "Survey and Characterization: Tidal In Stream Energy Conversion (TISEC) Devices," in *EPRI North American Tidal In Stream Power Feasibility Demonstration Project*.: EPRI, 2005.

[28] David R. Wilkinson, "A study of flow acceleration over a coastal headland," Oregon State University, Corvallis, MS Thesis 1979.

[29] H Sauvageot, *Radar Meteorology*. Norwood, Mass.: Artech House, 1992.

[30] Simon P. Neilla, Emmer J. Litta, Scott J. Couch, and Alan G. Daviesa, "The impact of tidal stream turbines on large-scale sediment dynamics," *Renewable Energy*, vol. 34, p. 2803–2812, June 2009.

[31] I.T. Jolliffe, *Principal Component Analysis*, 2nd ed.: Springer, 2002.

[32] NOAA National Geophysical Data Center. (2006, May) GEODAS Grid Translator - Design-a-Grid. [Online]. http://www.ngdc.noaa.gov/mgg/gdas/gd_designagrid.html

[33] Robert Stewart, *Introduction to physical oceanography*. Austin, 2008.

[34] Mirko Previsic and Rodger Bedard, "Methodology for conceptual level design of tidal in-steam energy conversion (TISEC) power plants," in *EPRI North American Tidal In Stream Power Feasibility Demonstration Project*.: EPRI, 2005.

[35] Adrian E. Gill, *Atmosphere-ocean dynamics*. San Diego: Academic Press, 1982.

[36] Lasse Gilling and Niels N Sørensen, "Large Eddy Simulations of an Airfoil in Turbulent Inflow," in *4th PhD Seminar on Wind Energy in Europe*, Aalborg, Denmark, 2008.